# I. THE THERMAL CONDUCTIVITY MEASUREMENTS OF SELECTED SILICATE POWDERS IN VACUUM FROM 150°-350°K

# II. AN INTERPRETATION OF THE MOON'S ECLIPSE AND LUNATION COOLING AS OBSERVED THROUGH THE EARTH'S ATMOSPHERE FROM 8-14 MICRONS

Thesis by

Kenneth Watson

In Partial Fulfillment of the Requirements

For the Degree of

Doctor of Philosophy

California Institute of Technology

Pasadena, California

1964

# ACKNOWLEDGMENTS

In the course of this research the writer has incurred many debts of gratitude which, it is hoped will be repaid in some small measure by its completion.

Dr. Harrison Brown, the writer's research advisor, has provided assistance and encouragement through the course of this investigation.

The good counsel and stimulation of Dr. Bruce Murray is deeply appreciated. The writer's interest in this problem are a direct result of the research in which Dr. Murray has been actively engaged.

Dr. Robert Wildey has given unstintingly of his time, knowledge and friendly support. In particular he has devoted a considerable effort in critically reviewing those aspects of this study related to radiative transfer.

The assistance of Mr. Curtis Bauman during the construction of the thermal conductivity apparatus was invaluable. His ingenuity and experience played a major role in the completion of this aspect of the investigation.

The writer wishes to thank Mr. Jim Westphal for his helpful suggestions during the design of the apparatus.

The secretarial assistance of the writer's wife, Norma Watson, during the preparation of this manuscript is gratefully acknowledged.

## ABSTRACT

An apparatus was constructed to measure the thermal conductivity of powders in vacuum from 150° to 350°K. It was found that the conductivity of selected silicate powders can be adequately represented, within the experimental errors, by a temperature independent term related to the contact conduction plus a temperature cube term which is due to radiative transfer between and through the grains. The conductivity for glass spheres approximately suggests an inverse grain size dependence and does not appear to be related in any simple manner to the elastic contact area between the spheres. The effects of angular grains, produced by crushing, and limited chemical composition range are not significant when compared with the experimental errors. The radiative transfer term which is grossly independent of chemical composition and grain texture is dominated by radiation between the grains for grain sizes $> 300\ \mu$. Radiation through the grains is significant for grain sizes $< 100\ \mu$.

Previous interpretations of the eclipse observations of Pettit and Nicholson indicate that homogeneous constant thermal property models provide an adequate fit. The recent lunation observations of Murray and Wildey cannot be adequately explained by homogeneous models with either constant thermal properties or with thermal properties which are based on the results of this experimental investigation and existing specific heat data. It is suggested that the possibility of layering can best be examined in the region of the morning terminator.

TABLE OF CONTENTS

# PART I. THE THERMAL CONDUCTIVITY MEASUREMENTS OF SELECTED SILICATE POWDERS IN VACUUM FROM 150° TO 350°K

## 1. INTRODUCTION

The thermal conductivity of powders in vacuum was originally of interest in the manufacture of highly insulating dewars for the storage of low temperature fluids. With the recently renewed interest in lunar geophysics, the infrared emission from the Moon's surface as observed through the Earth's atmospheric transmission window from 8-14 μ has assumed new significance.

The primary purpose of the first part of this investigation was to establish whether radiative conduction in selected silicate powders in vacuum was sufficiently large over the temperature range encountered on the lunar surface to produce a significant departure from the theoretically computed cooling curves which have assumed a thermal conductivity which is independent of temperature. It was also considered desirable to compare the observed cooling curves with theoretical models based on the measured conductivities of various silicate powders.

The first part of this investigation involved the construction and use of an apparatus to measure the thermal conductivity of powders in vacuum. The earliest measurements (Smoluchowsky, 1910, Kannuluik and Martin, 1933; Aberdeen and Laby, 1927) of thermal conduction through powders were, in reality, a study of the conduction of various gases as a function of pressure down to $10^{-1}$ to $10^{-2}$ torr. One technique generally employed in thermal conductivity measurements of porous material (Jakob, 1949) is to use a heating element to provide a known flux

and measure the resulting temperature gradient in the sample with thermocouples. In the present study it was felt that this technique was inadequate for two reasons: (1) the difficulty of providing an accurately measured heat flux source at low temperatures, and (2) the distortion of the temperature gradient in the sample due to the presence of thermocouples with an appreciable conduction relative to the powder itself. Recently, (Cline and Kropshot, 1963) measurements have been made with a 1" powder sample bounded by walls at 77°K and 300°K. The resulting heat flux was measured by the rate of evaporation of cryogenic fluid. However, no attempt was made in that study to determine the thermal conductivity of the samples.

## 2. APPARATUS TO MEASURE THERMAL CONDUCTIVITY OF POWDERS IN VACUUM

An apparatus enclosed in a sand-cast aluminum vacuum chamber capable of retaining pressures of $10^{-5}$ to $10^{-6}$ torr was used to measure the thermal conductivity of powder samples in vacuum (fig. 1). The base of the sample was heated by the temperature bath on which it rested. The top surface of the sample radiated into a cavity which was maintained at liquid nitrogen temperature (77°K). The thermal conductivity of the powders was calculated from the emitted flux, the sample thickness, and the bath temperature.

The construction and operation of this apparatus has been described in detail (Watson and Bauman, 1963). The flux emitted from the sample surface into the liquid nitrogen cavity was observed through a cooled f/16 aperture and chopped by a liquid nitrogen cooled black chopper blade. The resulting modulated flux passing out of the bell jar was measured by an 8-14 μ filtered infrared photoconductor photometer. The mercury doped germanium photoconductor and related instrumentation used in these measurements has been described by Westphal, Murray and Martz (1963). The doping of the germanium crystal with mercury atoms extends its long wavelength cutoff from 1.8 μ (1.45 ev) to 13.5 μ (10.9 ev). A short wavelength cutoff of 8.5 μ (6.85 ev) is provided by an interference filter. The use of liquid hydrogen reduces the density of both thermal electrons present in the crystal and electrons liberated by the unmodulated flux of photons emitted by the surrounding surfaces. The A.C. variations in the cell resistance produced by the modulated flux are measured by providing a battery-generated

FIGURE ONE

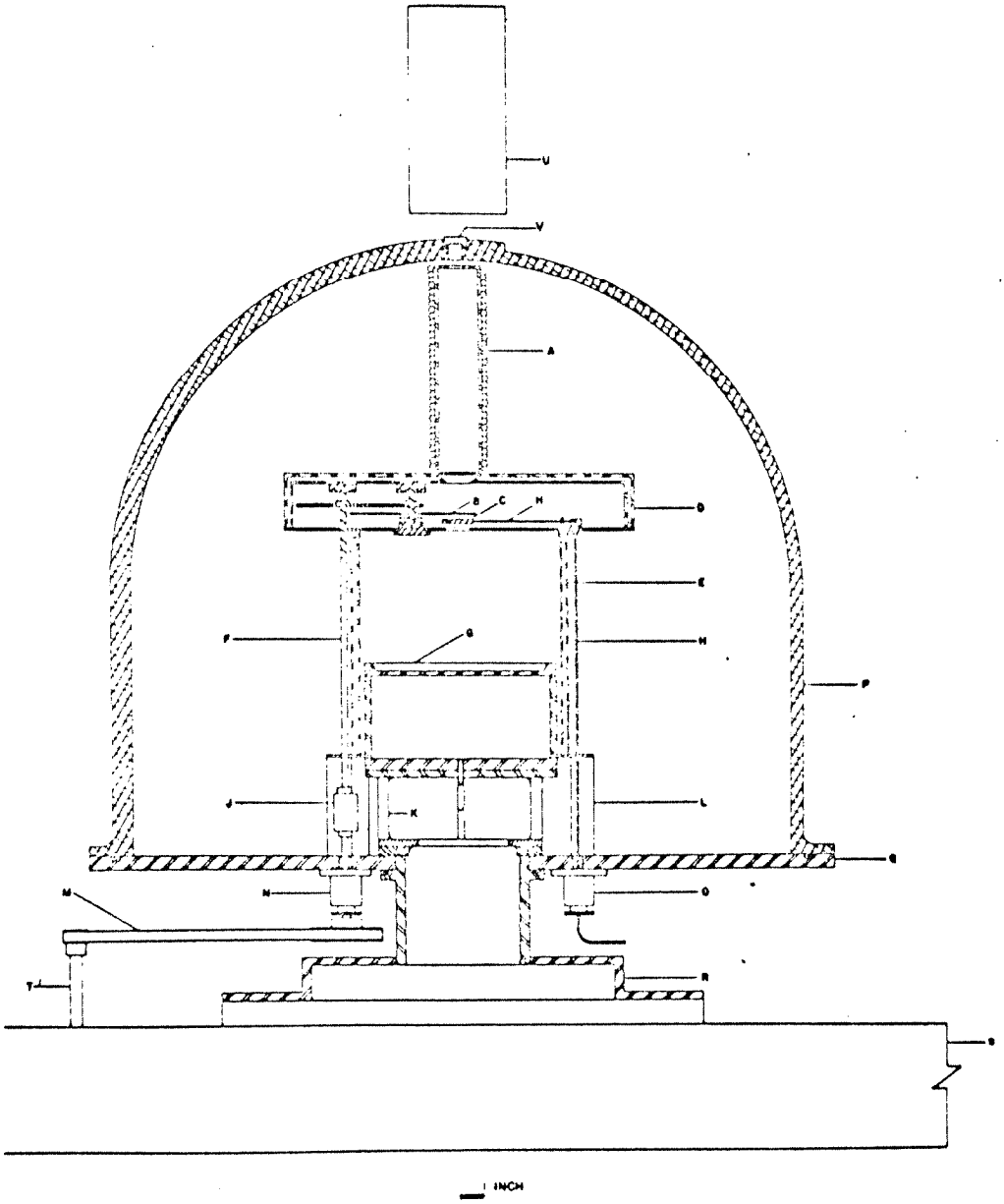


Thermal conductivity apparatus (A) aperture shield, (B) chopper blade, (C) calibration device, (D) upper liquid $N_2$ chamber, (E) lower liquid $N_2$ chamber, (F) drive shaft, (G) temperature bath (H) calibration inlet and outlet lines, (J) bellows coupling, (K) temperature bath stand, (L) Lucite leg, (M) timing belt, (N) rotary seal, (O) rotary seal, (P) vacuum chamber, (Q) base plate, (R) sub chamber, (S) pumping station, (T) synchronous motor shaft, (U) infrared detector, (V) KRS 5 window

current through the cell and amplifying the resulting voltage signal.

A reference calibration unit was installed between the sample and the chopper system so that the sample flux could be compared with the flux from a black body at a known temperature. It was found necessary to install this unit because of long-term detector response variations. The bath and calibration temperatures were measured external to the vacuum chamber by thermometers inserted in the inlet and outlet fluid lines.

## 3. SAMPLE PREPARATION AND HANDLING

It was decided to restrict the experimental study to silicate powders for two reasons: (1) over 90% of the terrestrial igneous rocks are composed of silicates (Dana, 1955), and (2) the similarity between the Moon's mean density of 3.34 $gm/cm^3$ and the density of iron-magnesium silicates. The high silicate composition of meteorites provides further evidence that silicates are likely to be the main constituents of the surfaces of the inner planets and the Moon.

Quartz, silica glass, olivine and hornblende were used as representative samples to determine the gross effects of composition on the powder conductivity. The silica glass was obtained commercially in the form of microbeads (round spheres) of varying grain size ranges: 840-590 μ, 350-250 μ, 125-88 μ, 74-53 μ, and less than 37 μ. For comparison of the effects of crushing, the largest microbeads were crushed down to a 74-44 μ range. The quartz, olivine, and hornblende samples were all crushed and sieved below 74 μ, and a second quartz sample was prepared between 74-44 μ. Appendix I contains a more detailed description of the samples and the crushing procedures used.

A sample run was performed by pouring a known weight of sample carefully onto the temperature bath and striking the sides of the bath to produce a uniformly flat surface. It was decided that reproducible packing would be important so care was taken to treat all samples in as consistent a manner as possible and attempt to attain high packing in all cases. Looser packing would introduce severe problems in the non-uniformity of the sample surface and local variations in the sample thickness.

The possibility existed, also, that adsorbed water might be retained in the powder samples even under the low pressures attained during the experimental runs ($10^{-5}$ to $10^{-6}$ torr). To examine this effect several samples were placed in a glass tube and connected to the vacuum pump. After being degassed for 24 hours (as was done in the case of all experimental runs) the tube was heated with an open flame. There was no indication of a change in the sample packing nor gas release as might be evidenced by the sample surface or by changes in the measured pressure. As a second test, several experimental runs were repeated with degassing times of three or four days. No measurable changes in the conductivity were observed. The results of Roddy et al. (1962) on the effects of rapid degassing and sample heating on the packing of thick powder samples indicated that it was possible to degas a sample without heating provided that the initial degassing rate was low and that the total pumping time was several hours. None of the present author's sample surfaces showed any indication of disruption following the conductivity measurements.

Sample thicknesses were measured by a very simple operation suggested by J. A. Westphal. A microscope was focussed on the bath surface before the sample was added. Then the microscope was refocussed on the sample surface and the resultant vertical movement of the microscope tube measured. The center sample thickness and the mean sample thickness (used in the density calculations) were determined by repeated measurements at the center and edges. The effect of differences between the center and mean thicknesses will be discussed in section 5.1 in the error analysis.

## 4. DATA REDUCTION

The sample thickness, bath temperature and calibration temperature are direct measurements discussed in the previous sections. The sample densities were computed from the mean sample thickness, the sample weight, and the area of the bath surface.

The brightness temperature* response curve for the cell was initially determined by numerically integrating the measured spectral response of the detector with the Planck function.

$$S(T) = \int_0^\infty r(\lambda) B(\lambda, T)\, d\lambda \qquad (1)$$

where

$r(\lambda)$ = detector response

$$B(\lambda, T) = \frac{C_1}{\lambda^5} \frac{1}{\ell^{C_2/\lambda T} - 1}$$

$C_1 = 3.741 \times 10^5$ erg/cm$^2$/sec

$C_2 = 1.439$ cm. deg.

$\lambda$ = wavelength in cm.

$T$ = temperature in °K

The resulting computed curve was then checked at a few temperatures by removing the sample and measuring the flux emitted by the surface of the bath. The agreement was sufficiently accurate to

---

*The brightness temperature of an object is defined as the temperature of a black body cavity emitting the same flux as the object over a specified spectral region.

permit the use of the analytically computed response curve to determine the brightness temperatures of the sample surface.

We shall simplify our initial discussion of the determination of the sample thermal conductivity by assuming that the sample is homogeneous, that the flux emitted by the sample is Planckian in distribution, that this flux originates at the top surface of the sample, and that the sample is sufficiently wide in comparison to its thickness that the heat flow is one-dimensional. Then,

$$\frac{\partial}{\partial x}\left(K(T)\frac{\partial T}{\partial x}\right) = \rho C(T)\frac{\partial T}{\partial t} \tag{2}$$

$$-K(T)\frac{\partial T}{\partial x}\bigg|_{x=L} = \sigma T^4\bigg|_{x=L} - \sigma T_W^4 \tag{3}$$

$$T\big|_{x=0} = T_B \tag{4}$$

where the distance $x$ is measured up from the surface.

$T = T(x,t)$ temperature

$K = K(T)$ thermal conductivity

$\rho$ = sample density

$C = C(T)$ specific heat

$\sigma$ = Stefan Boltzmann constant

$T_W$ = effective temperature of the cavity walls ($\sim 77°K$)

$L$ = sample thickness

$T_B$ = bath temperature

The time-dependent solution for the surface temperature involves

the temperature variation of the conductivity and specific heat, and the initial temperature distribution. It was felt that the steady state solution which is independent of the initial temperature and the specific heat would provide a more reliable estimate of the conductivity function. Since equilibrium cannot be attained experimentally the assumption was made that when the surface brightness temperature did not change by a measurable amount during one hour an effective steady state exists. A discussion of the error involved will be found in section 5.3.

The steady state solution for the surface temperature is expressed in the integral equation:

$$\int_{T_L}^{T_B} K(T)\, dT = \sigma(T_L^4 - T_W^4) \cdot L \qquad (5)$$

where $T_L$ is the surface temperature (since our assumptions require that the effective, brightness, and surface kinetic temperatures be equal).

By repeating this experiment for the same sample but with different bath temperatures we obtain a set $(T_B, T_L)$ for the same sample thickness.

The mean conductivity can be defined by

$$\overline{K} = \frac{\sigma(T_L^4 - T_W^4) \cdot L}{T_B - T_L} = \frac{1}{T_B - T_L} \int_{T_L}^{T_B} K(T)\, dT \qquad (6)$$

Consolidated materials have fairly large conductivities and hence small temperature gradients result in large heat fluxes. Thus, even when the conductivity has a non-linear dependence on temperature, the mean conductivity defined as above does not differ appreciably from the conductivity at the mean sample temperature.

Powders in vacuum, on the other hand, cannot be characterized by a mean conductivity $\overline{K}$ for two reasons: their low conductivities require large temperature gradients to provide measurable fluxes, and the radiative conduction between the grains is dependent, to the first order, on the temperature cubed. In this case it is clear that the mean conductivity and the conductivity at the mean temperature may differ by a significant amount.

A variety of analytical expressions for $K(T)$ can be chosen and the standard deviations examined to determine the best fit. A second approach is to determine an appropriate physical model for the conductivity and then use the experimental results to determine the numerical constants. The latter approach has the significant advantage that one can attach physical meaning to these numerical constants, and it is this method which will be primarily utilized in this investigation.

## 4.1 First Order Theory

We shall consider a simple model which assumes that the sample conductivity is the linear sum of two parts: a solid conduction term which is independent of temperature, and a radiative conduction between the grains. This latter term has a temperature cubed dependence as can be illustrated in the following manner. Consider two flat sheets which have emissivities $\epsilon$, are connected to temperature baths at $T_1$ and $T_2$, and are separated by a distance $L$. If there is a vacuum between the surfaces then the net heat flow from surface 1 to surface 2 (if $T_1 > T_2$) can be expressed as

$$q_{net} = \frac{\epsilon\sigma}{2-\epsilon}(T_1^4 - T_2^4) \qquad \text{(Jakob, 1949)} \qquad (7)$$

We can define an effective conductivity as follows:

$$q_{net} = K_e\left(\frac{T_1 - T_2}{L}\right),$$

$$\therefore \quad K_e = \frac{\epsilon\sigma}{2-\epsilon}\left(\frac{T_1^4 - T_2^4}{T_1 - T_2}\right) \cdot L$$

If $T_2 = T_1 - \Delta T$ and $\Delta T \ll T_1$, then

$$K_e \sim \frac{4\epsilon\sigma T_1^3 \cdot L}{2 - \epsilon} \qquad (8)$$

Thus the first order theory assumes that

$$K(T) = AT^3 + B \qquad (9)$$

where A and B are numerical constants to be derived from the experimental measurements.

A temperature cubed dependence for the radiative conductivity can be derived at large optical depths provided that the opacity of the sample is independent of wavelength. The equations and assumptions necessary to obtain this result are presented in Appendix 2.

Equation 9 also provides a convenient form to estimate the relationship between radiative conduction and ordinary conduction through the solid, independent of sample thickness. The error introduced into equations 9 and 5 from the non-uniformity of the sample thickness can thus be minimized. The relevance of more refined expressions for the conductivity will be discussed in section 5.3.

# 5. ERROR ANALYSIS

There are three major sources of error in an analysis of the thermal conduction of powders in vacuum: (1) experimental errors resulting from measurements, (2) errors arising from non-reproducible sample packing, and (3) errors resulting from assumptions used to formulate the basic equations.

## 5.1 Experimental Errors

The experiment involved the measurement of the bath and calibration unit temperatures, the preamplifier signal, and the sample thickness and weight. By their nature the errors involved are the simplest to relate directly to the derived conductivity function. The errors resulting from the direct measurement of the temperature of the bath and calibration fluids arise from the fact that the actual temperatures of the surfaces involved are not measured directly but are chosen as the mean temperature of the inlet and outlet fluids. This assumption is probably justified since the calibration fluid cooled by less than 0.2 °K and the temperature bath by less than 2°K. The agreement between the measured and computed response curve suggests that these measurements are not a significant source of error. The error introduced by the bath temperature measurement is of the order of 1% of the computed conductivity. Errors introduced by the calibration temperature measurement effect the conductivity in a more subtle manner since they involve the brightness temperature. A change of 0.1°K in the calibration temperature will change the computed response at 300°K (normal operating temperature for the the calibration fluid) by less than 0.2%. In connection

with this discussion of the calibration and the bath surface temperatures it is instructive to compute the cooling of the fluid due to radiation emitted from these surfaces. A black body at 300°K emits $4.6 \times 10^5$ ergs/cm$^2$/sec. This is equivalent to the power given up by a cubic centimeter of water when cooled 0.01°K in one second. Since the area of the calibration unit is approximately 4 cm$^2$, a flow rate of 1 cm$^3$/sec will provide the required flux with a temperature drop of 0.05°K. The measured temperature drop of 0.2°K is in reasonable agreement with the actual flow rate and total area of the calibration unit and the feeder lines. Thus the mean fluid temperature and surface temperature of the calibration unit are in reasonably good agreement. A similar analysis for the temperature bath indicates that error introduced by neglecting the temperature gradient across the bath surface between the fluid and the sample is negligible.

The preamplifier signal errors were due to two sources: non-linearity in electrical response, and fluctuations in the signal due to the non-uniform modulation. The preamplifier was operated without any internal filtering due to the high signal to noise ratio (> 20:1). The non-linearity of the preamplifier scale was measured by using an oscillator with a 100 cps output signal, and recording the scale deflection for an input signal which was decremented in tenths of the full scale deflection. Repeated checks for non-linearity over several months did not indicate any measurable time dependence. The non-uniform signal modulation resulted from a slight wobble in the chopper blade system.

Errors introduced from the measurement of the sample thickness

were mentioned previously. Actually the only significant errors arose, not from an individual measurement which was accurate to 0.01 cm, but from lack of uniformity of the sample thickness requiring an average of several measurements. These variations indicated that the thickness varied by about 5% for samples thicker than 0.5 cm, and by as much as 10% for 0.2 cm sample thicknesses. This error was so large that the data reduction procedure was modified to compute the ratio of B/A as defined in equation 9, since this ratio can be determined independently of the sample thickness. A mean value of B/A was then computed for each sample material, and B and A for each set of temperatures was computed from the mean value of B/A.

The sample weight was measured to an accuracy of 0.1 gm. Clearly the error in the sample thickness overwhelmed this error in determining the sample density.

## 5.2 Reproducible Packing Errors

The sample packing was controlled only in a modest way by the attempt to treat samples in a similar fashion and approach a high degree of packing. The sample densities were measured to provide an indication of the degree of packing but since the value of B (ordinary solid conduction) will be shown to depend primarily on the particle contacts, it is clear that the density measurements provide a rather tenuous indication of the reproducibility of the packing state. Differences in the packing state for the experimental runs performed on the same sample material are probably the major source of variations in the ratio B/A.

5.3 Errors Introduced by Assumptions

The initial assumptions introduced in the analysis were that the heat flow could be treated as one-dimensional and steady state. To examine these assumptions it is justifiable to neglect the temperature variation of the conductivity and choose a minimum value which will tend to overemphasize both effects. The assumption of one-dimensional heat flow was examined by calculating the steady state solution for a cylinder whose bottom and side temperatures were equal to the bath temperature and whose surface radiated into free space. A ratio of cylinder height to radius was chosen similar to the samples run (1:20). The computed variation of surface temperature over the area of the sample viewed by the detector is less than 0.5°K for an assumed conductivity of 100 ergs/cm/sec/deg. Again it must be concluded that the errors introduced by the non-uniformity of the sample thickness are in excess of any errors introduced by assuming one-dimensional heat flow. The assumption of steady state equilibrium was examined both from computed cooling rates and by comparing the measured brightness temperature when the sample was warming up from a cooler temperature, with that when the sample was cooling down from a warmer temperature. The differences in the measured brightness temperatures were less than the experimental errors discussed previously. The computed cooling rates were calculated assuming one-dimensional heat flow in a sample whose thermal properties are independent of temperature. The resulting curves indicate that the length of time taken for the experimental measurements was

sufficiently long to measure the conductivity within the accuracy of experimental errors.

In equation 5 the assumption is made that the brightness, effective, and surface kinetic temperatures are all equal. This assumption is justified within the experimental accuracy of our measurements by the high opacities of silicates indicated by Launer's data (1952) and the emissivity measurements of Burns and Lyons (1963). The high opacities (ranging from 100 to 1000 $cm^{-1}$ in the 8-14 $\mu$ region) fulfill the requirement that the contribution to the surface flux from radiation emitted at depth is negligible. The effect of the departure from unit emissivity and the variation with wavelength can be examined as a function of grain size using Burns' and Lyons' data for quartz and quartz sand. The most significant result of crushing the mineral is to reduce its high degree of reflection because of the multiple reflections off the randomly oriented particle surfaces. In Appendix 3 these emissivity curves have been used to examine differences between the surface kinetic temperature, the brightness, and the effective temperatures when the sample is opaque. The resulting changes in A and B are well below the experimental errors.

In section 4 two possible approaches to satisfying the integral equation 5 were discussed. The limitations imposed on both methods are a direct result of the sources of errors, since the ability to differentiate between models is in direct relation to the accuracy of this equation and the measured experimental quantities. The first method which involves the fitting of various algebraic expressions to the conductivity function provides a very simple method to examine the

possible variations with temperature. As a first approximation it was assumed that the conductivity is independent of temperature for each set of bath and surface temperatures. The mean conductivity versus the mean temperature was plotted for each set of measurements in each sample run. It was found that the mean conductivity decreases when the temperature decreases. This clearly demonstrates that the required form for the conductivity function must increase with increasing temperature. The conductivity function was then fitted with a linear dependence on temperature. The resulting expression has a negative value for the conductivity when the curve is extrapolated to 100°K or less. Thus the conductivity function must be fitted with temperature dependent terms some of which have powers greater than unity. The first order approximation to the conductivity function satisfies this criterion. The attempt to fit the conductivity function to quadratics, general cubics and higher order terms did not reduce the standard error of the least squares fit sufficiently to justify applying the numerical approach to obtain greater precision. The physical theory attack, however, permits an examination of the degree of departure from the model that the observational errors in the data justifies. The assumption of a simple constant plus cubic dependence implies that the contact conduction between the grains is temperature independent and that the radiation absorption coefficient of the sample is independent of wavelength. The former assumption is, by its nature, simply an educated guess. An accurate determination of the possible variation of the constant conduction with temperature would require measurements at much lower temperatures where the radiative

transfer is small. Even at moderately low temperatures, say 100°K and less, there is no guarantee that the transparency of the sample at very long wavelengths (> 100 μ) might not in fact provide a significant radiative transfer term. The major problem in attempting to attain low surface temperatures (< 150°K) with the described apparatus is that the samples must be thicker than 1 cm. The required times to achieve the criterion used for steady state equilibrium become days rather than hours. The need to provide liquid nitrogen every eight hours made this experiment unfeasible with the present apparatus. It is felt that assuming a temperature independent contact conduction is not too gross an oversimplification. The inability to reproduce the sample packing is probably a more significant source of error than the assumption of no temperature dependence.

The bulk opacity of the sample is assumed to be independent of wavelength. Some data is available on the transmission through fine particles from 1 μ to 15 μ (Launer, 1952). The sample thickness was obtained only indirectly from the stated sample density since he was interested only in relative variations of the transmission, but opacity values of the order of 100 $cm^{-1}$ are suggested for these results. The variations of opacity with wavelength were relatively small compared with the opacities computed from the results of this experimental study. It was assumed that a Rossland mean (see Appendix 1) could be used to examine what effect the opacity variations have on the temperature cubed dependence. Clearly a low opacity at short wavelengths will produce a greater radiative conduction at high temperatures than a temperature cubed dependence based on a mean opacity. It is also

clear that variations from a constant opacity generally cannot be represented by a simple $T^m$ dependence for the radiative conduction term. It is felt that these variations in mean opacity of a few per cent fall below the experimental errors involved both for the present lunar observations and the powder conductivity study. This is due primarily to the fact that low opacities over a narrow wavelength band will have a relatively insignificant effect on the bulk opacity since the flux involved is only a small fraction of the total flux.

## 6. EXPERIMENTAL RESULTS

In Appendix 4 the results of this experimental investigation are tabulated in terms of the directly measured quantities, i.e., sample thickness, weight, bath and calibration temperatures, calibration and sample signals. For conciseness only the final steady state results are listed. In this section the results are described in terms of the first order theory discussed previously. Three different bath temperatures were used for each experimental run.

From equations 5 and 9 we write

$$\frac{A}{4}\left[\frac{(T_B^{IJ})^4 - (T_L^{IJ})^4}{T_B^{IJ} - T_L^{IJ}}\right] + B = L_j\sigma\left[\frac{(T_L^{IJ})^4 - T_W^4}{T_B^{IJ} - T_L^{IJ}}\right] \qquad (10)$$

where I refers to the single set of surface and bath temperatures obtained in run J, (I = 1, 2, 3).

For a particular sample material (i.e., same grain size, composition and texture) we obtain a mean value of B/A which is independent of the sample thickness $L_J$ as follows:

$$X^{IJ} \equiv \frac{(T_B^{IJ})^4 - (T_L^{IJ})^4}{4(T_B^{IJ} - T_L^{IJ})} \qquad I = 1, 2, 3$$

$$Y^{IJ} = \frac{\sigma[(T_L^{IJ})^4 - T_W^4] \cdot L^J}{T_B^{IJ} - T_L^{IJ}}$$

$$Z^{KJ} \equiv \frac{Y^{KJ} \cdot X^{3J} - X^{KJ} \cdot Y^{3J}}{Y^{3J} - Y^{KJ}} \qquad K = 1, 2$$

$$\therefore (B/A)_{mean} = \sum_{J=1}^{\bar{J}} \frac{(Z^{1J} + Z^{2J})}{2\bar{J}}$$

For each set we can obtain values of $B_{IJ}$ and $A_{IJ}$ and thus determine a mean value for B and A separately as follows:

$$A^{IJ} = \frac{Y^{IJ}}{X^{IJ} + (B/A)_{mean}}$$

$$B^{IJ} = A^{IJ} \times (B/A)_{mean}$$

The results are plotted in figures 2 through 7 and tabulated in Appendix 4. The ratio $(B/A)_{mean}$ is plotted with the standard deviation indicated on the ordinate and the grain size range on the abscissa. A and B are the mean values of $A^{IJ}$ and $B^{IJ}$, and are plotted with their deviations.

FIGURE TWO

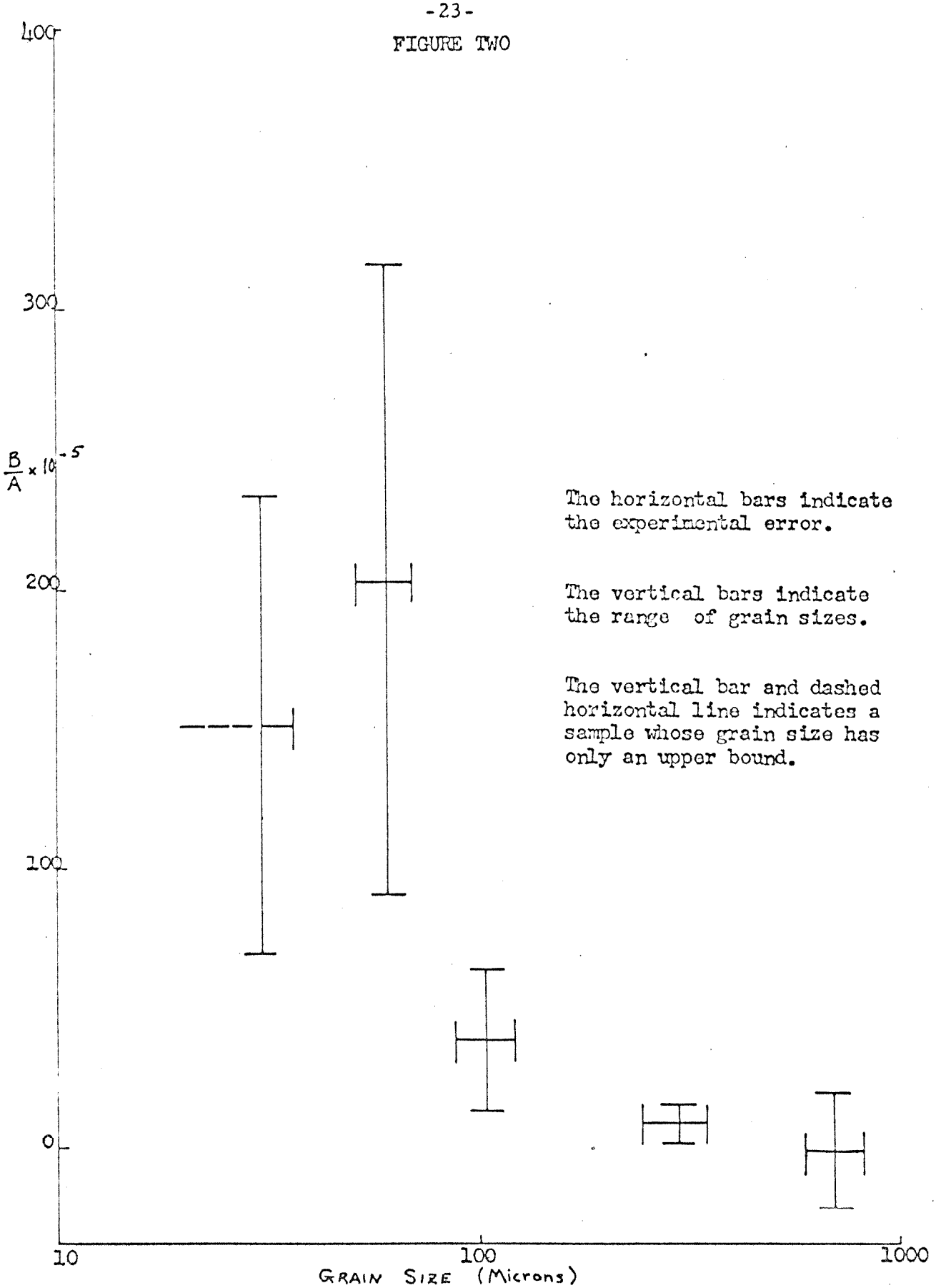


The Ratio B/A As a Function of Grain Size for Glass Spheres

FIGURE THREE

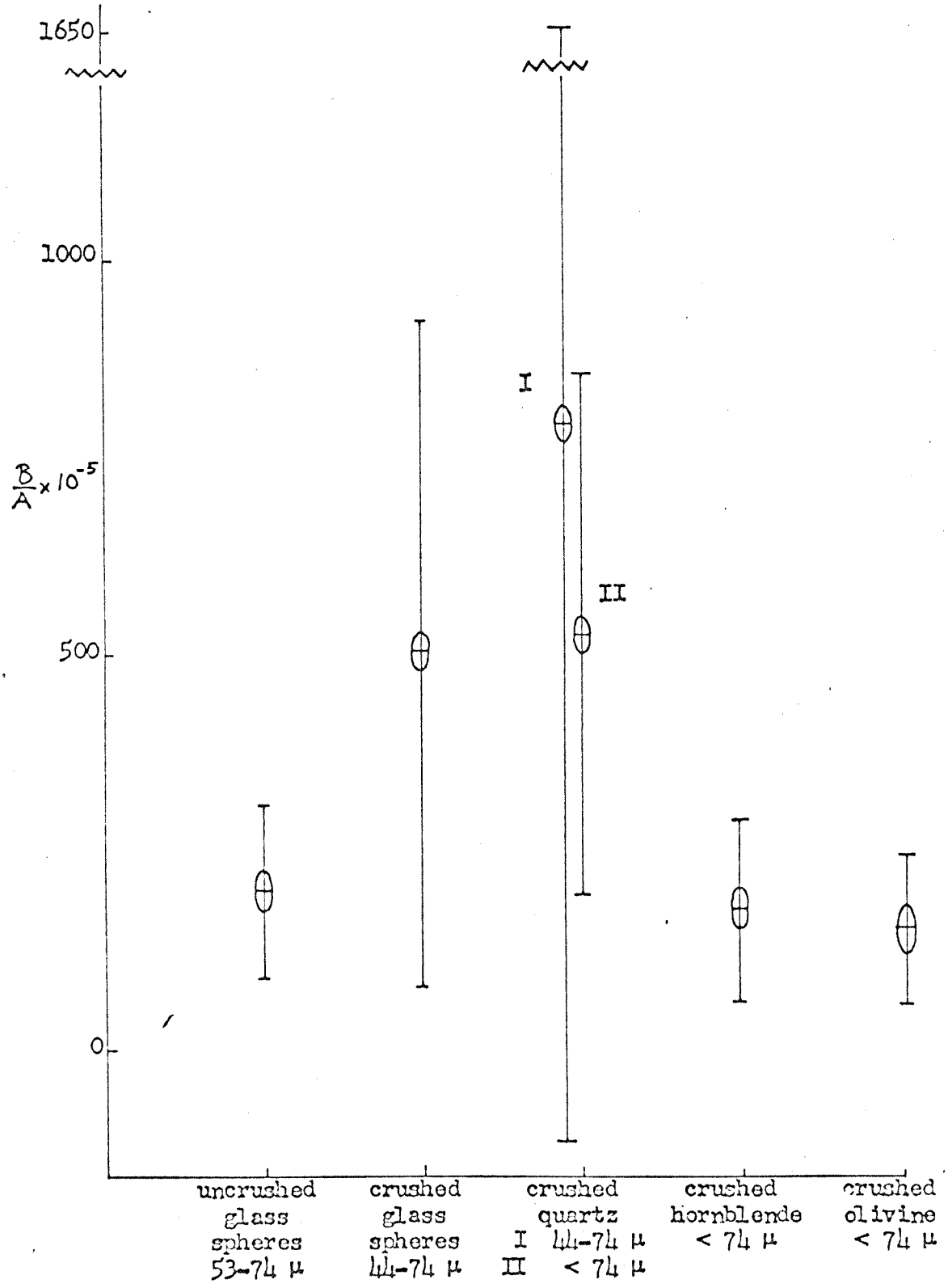


The Ratio B/A As a Function of Chemical Composition and Grain Texture

FIGURE FOUR

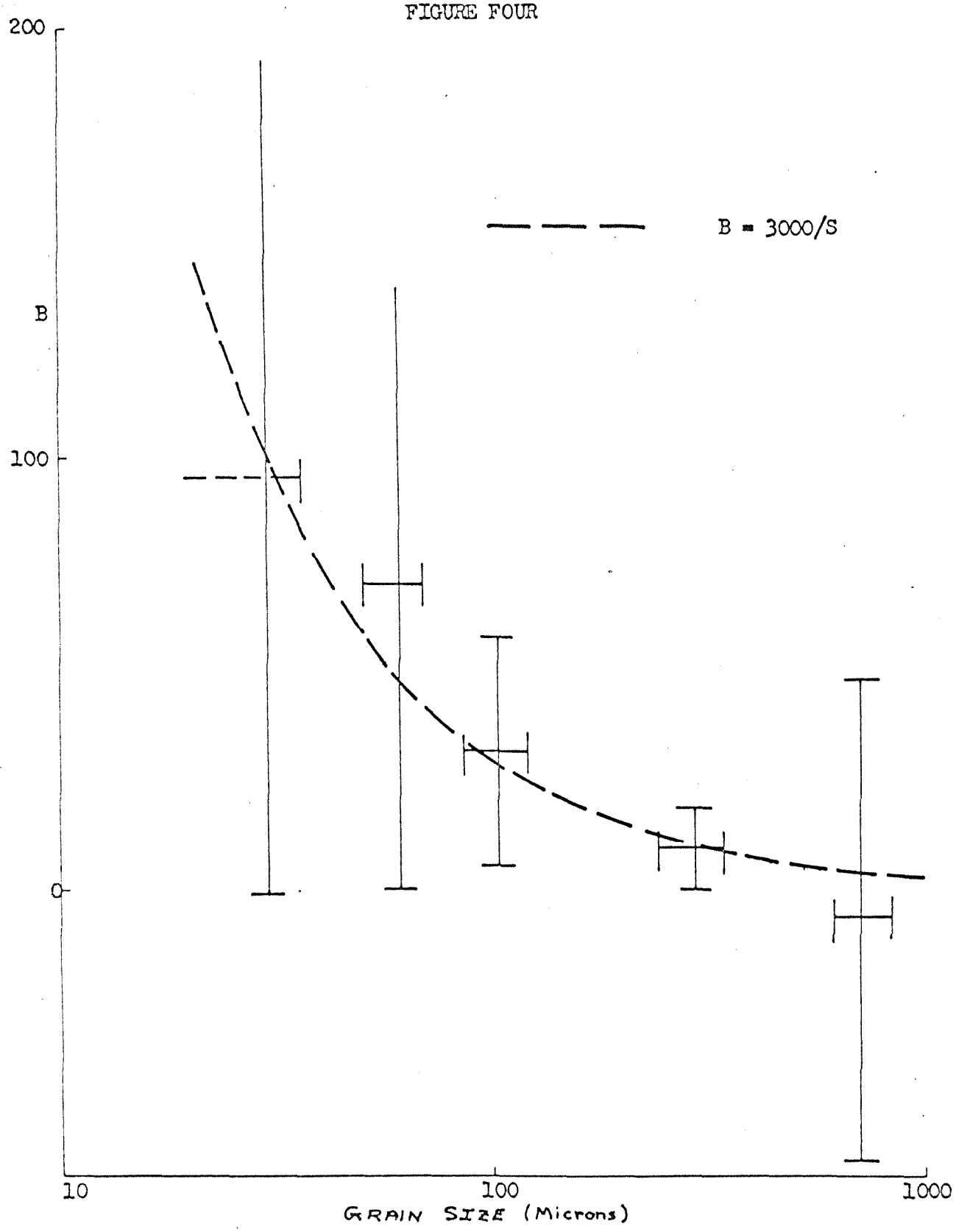


Contact Conduction, B, As a Function of Grain Size for Glass Spheres

FIGURE FIVE

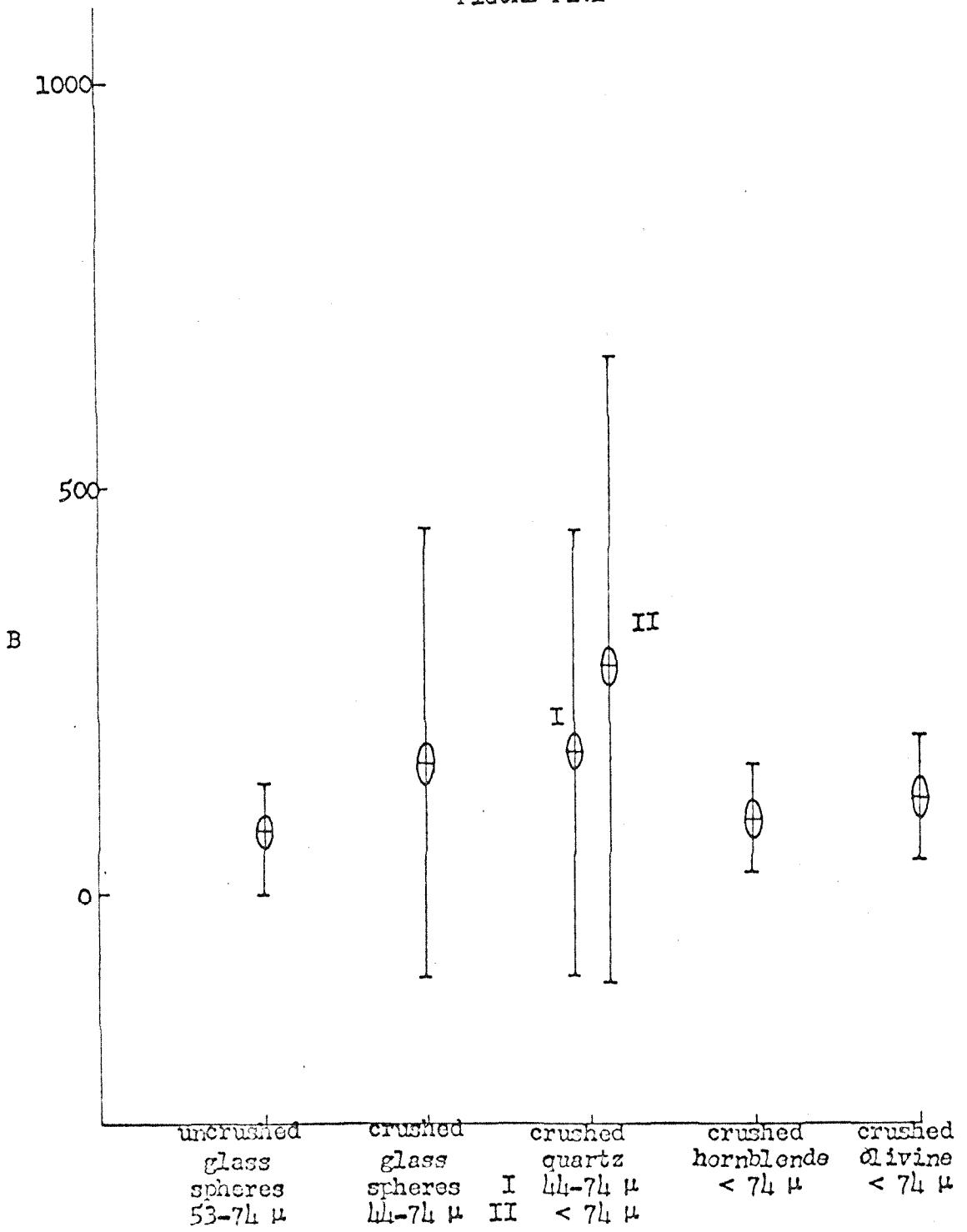


Contact Conduction, B, As a Function of Composition and Grain Texture

FIGURE SIX

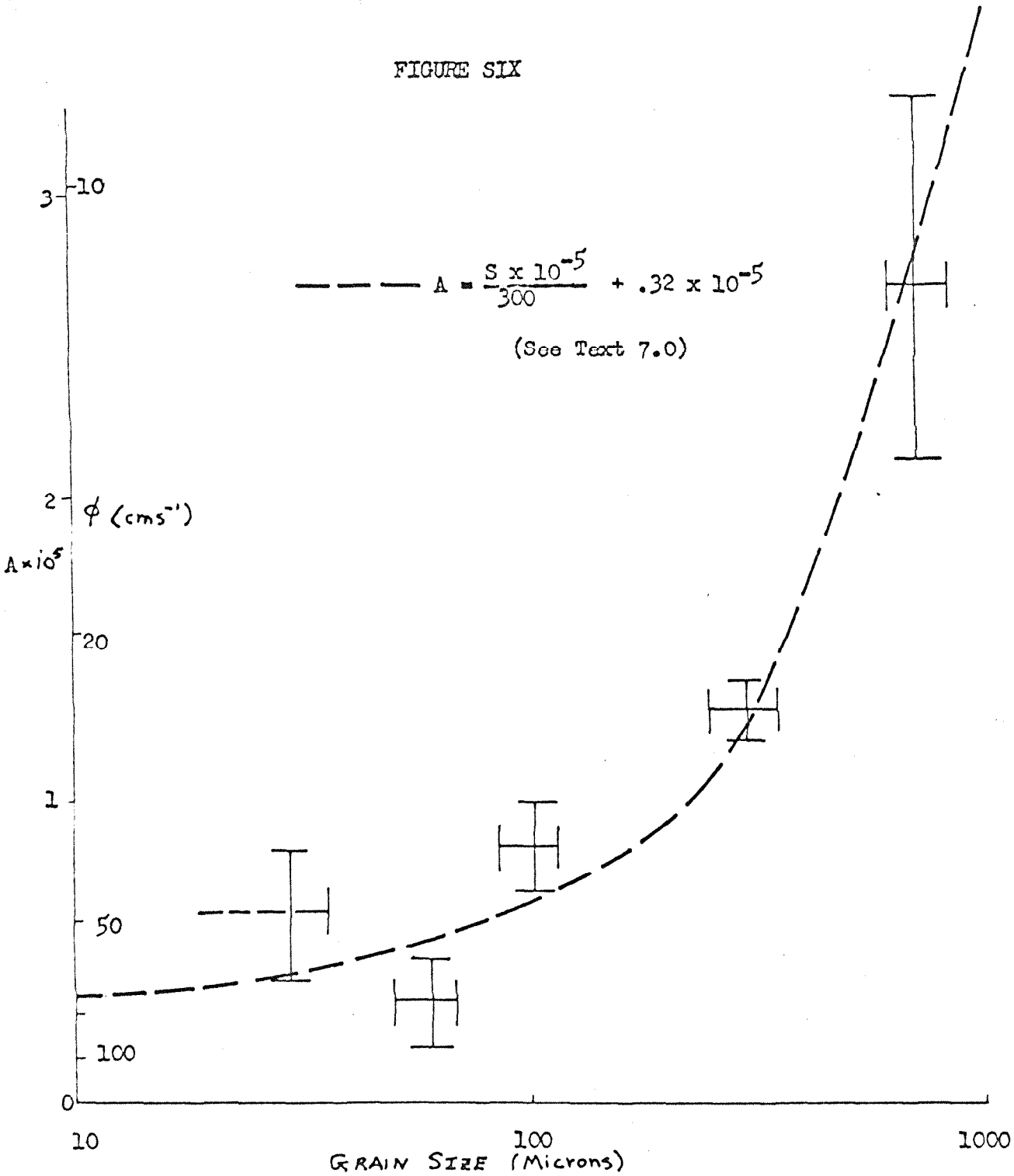


The Radiative Transfer Coefficient, A, and The Bulk Opacity, $\phi$, As A Function of Grain Size For The Glass Spheres

FIGURE SEVEN

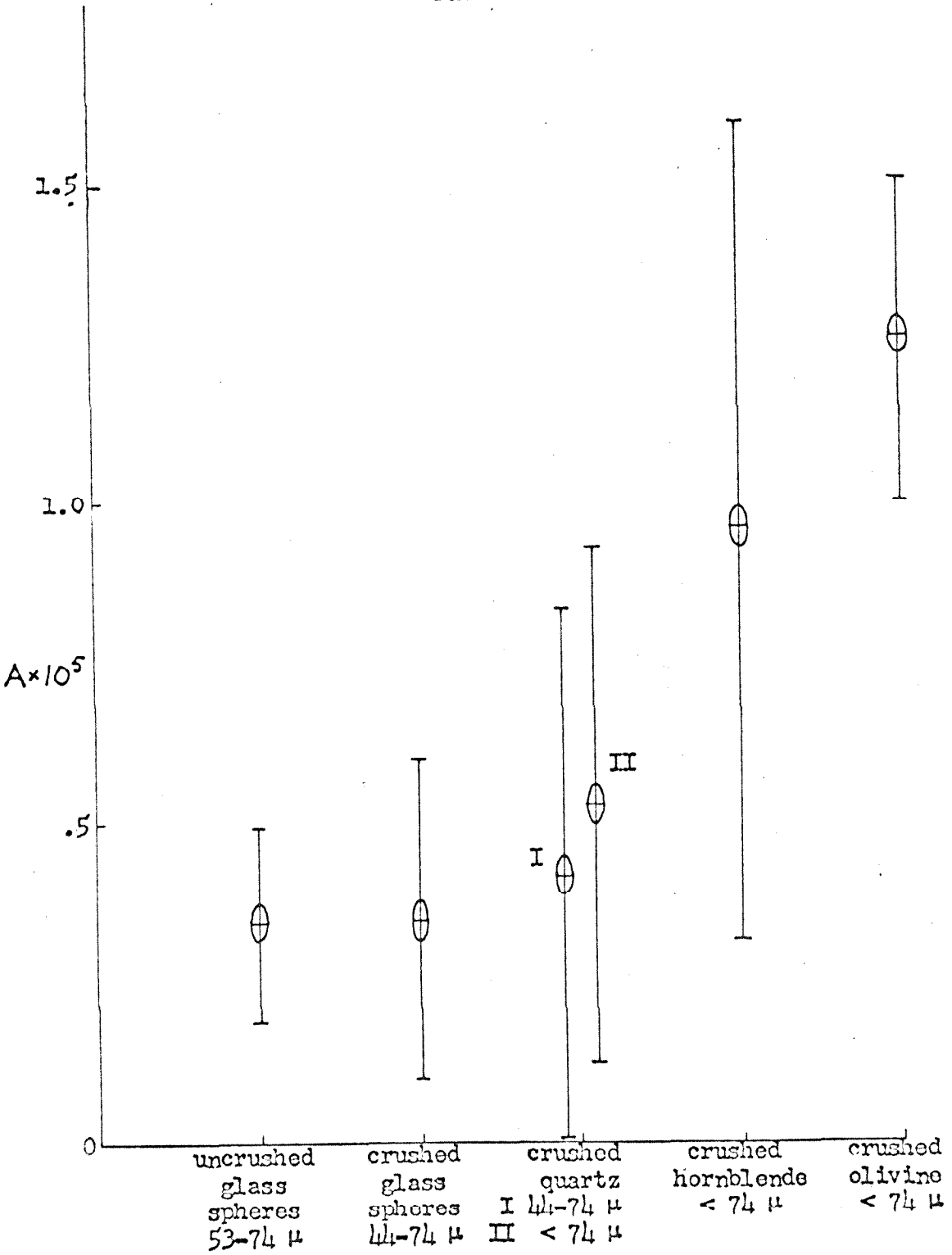


The Radiative Transfer Coefficient, A, As A Function of Chemical Composition and Grain Texture

## 7. PHYSICAL INTERPRETATION

The contact conduction term will be discussed initially. Since the solid conduction for silica glass is $\sim 1 \times 10^5$ ergs/cm/sec/deg it is clear that a grain conduction of 100 ergs/cm/sec/deg or less cannot be explained simply by the lower bulk density. The effect must be due primarily to the small contact between particles, which has a sufficiently high thermal resistance, to reduce the conductivity by a factor greater than 100. This is, in fact, the major reason why no attempt was made to relate the possible temperature dependence of the bulk solid (for a glass the conductivity decreases approximately linearly with temperature (Birch, 1942) ).

In Appendix 5 the circle of contact from the loading of elastic spheres (Hertz, 1881) is computed. A comparison of the contact resistance for a welded surface contact with the experimental results indicates that this computed contact resistance is lower by an order of magnitude for grain sizes $> 100\ \mu$ than the results indicated from the powder measurements. The variation of contact resistance with grain size does not appear to fit the grain size dependence of the simple theory outlined above. We must conclude that the interface between the spherical grains is not a welded contact and that the effective cross section of the contact is much smaller than the cross section bounded by the circle of contact. The irregularity of this contact will be affected by the non-sphericity of the particles, and their microscopic roughness. It is also possible that the reflection of elastic energy from this interface and surface chemistry effects will contribute to the

higher thermal impedance. The contact conduction can be approximately fitted to an inverse grain size dependence. This variation can be explained if the effective contact area is independent of grain size and compressive force.

The angular grains resulting from crushing have a slightly higher contact conduction than the uncrushed microbeads since their irregular shapes provide a larger number of contact points than do the spheres of the same grain size. Figure 6 indicates that no significant variation in contact conduction with chemical composition is observed. This is presumably related to the grossly similar behavior of these solids when being crushed to small particles.

Figures 6 and 7 illustrate the variation of bulk opacity as a function of grain size and composition. The compositional effect is masked by the experimental errors and will be treated as insignificant. The grain size dependence of the glass spheres suggests two possible effects: an increasing opacity with decreasing grain size due to radiative transfer between the grains, and, for grain sizes less than 80 microns, the combined effects of radiative transfer between and through the grains. An approximate fit to the data was made by assuming that the bulk opacity approached 100 $cm^{-1}$ for decreasing grain size. The grain size dependent term was chosen to honor the experimental values as closely as possible. Equation 8 indicates that the radiative transfer between the grains should be approximately proportional to the grain size. The curvature of the grain surfaces and the irregularity of the packing precludes a more detailed examination of the grain size dependence. The excellent agreement between the radiative transfer through

the void spaces $\sim 3 \times 10^{-4} ST^3$ (where S is the grain size in cms) and the effective radiative conductivity defined in equation 8, i.e., $2.4 \times 10^{-4} \frac{\epsilon}{2-\epsilon} LT^3$ (L is the plate separation) is fortuitous. The variability in the packing state of the samples and the scatter of the data points is too large, and a geometric factor should be included in equation 8 to represent the shape of the grain surfaces. For grain sizes less than 80 microns the departure from the simple theory is probably due to the finite transparency of the grains. As the grain size becomes smaller the radiative transfer through the grains becomes a significant fraction of the total radiative transfer. For example, a material with an opacity of 100 $cm^{-1}$ will attenuate the flux by a factor of 0.91 in 10 microns, 0.37 in 100 microns, and 0.05 in 300 microns. It is clear that radiative transfer through the grains is significant only at small grain sizes.

# 8. CONCLUSIONS

This investigation of the thermal conductivity of selected silicate powders in vacuum indicates that the conductivity can be adequately represented, within the experimental accuracy of the measurements, by a temperature independent term related to the contact conduction between the grains plus a temperature cubed term which is due to the radiative transfer between and through the grains.

The study of the thermal conductivity of the glass spheres indicates that the thermal contact between spheres is grossly independent of grain size and compressive force for the grain sizes from 30 $\mu$ to 800 $\mu$ and for sample thicknesses less than a centimeter. The contact conduction for the glass spheres can thus be approximated by an inverse grain size dependence. The crushed samples tended to have a somewhat higher contact conduction than spheres of the same grain size, however the large experimental errors in the derived contact conduction term, due to lack of uniformity in packing, prevents any detailed analysis of the effects of grain texture or chemical composition.

The radiative transfer term for the glass spheres suggests that a simple model can be derived in which the radiative transfer at grain sizes $> 300\ \mu$ is dominated by radiation through the pores and at grain sizes $< 100\ \mu$ has a significant contribution from radiation through the grains. The dependence of radiative transfer on the sample texture and chemical composition is not significantly apparent when compared with the experimental errors.

# PART II. AN INTERPRETATION OF THE MOON'S ECLIPSE AND LUNATION COOLING AS OBSERVED THROUGH THE EARTH'S ATMOSPHERE FROM 8-14 MICRONS

## 1. INTRODUCTION

The earliest attempts to measure the lunar infrared emission (Rosse, 1869; Langley, 1887) indicated that the maximum surface temperature was about 370°K. The first reliable measurements of the emission during the daytime portion of lunation and during an eclipse were made by Pettit and Nicholson (1930) in 1927. Pettit (1940) remeasured the eclipse cooling in 1939. Their measurements were made with a vacuum thermocouple placed at the Newtonian focus of the 100-inch telescope. The galvanometer deflections were calibrated by measuring the shorter wavelength signal from comparison stars and extrapolating both the stellar radiation and thermocouple response to the 8-14 μ region. Several filters were used to measure the flux received over different wavelength regions. The authors concluded that the rapid surface cooling of the Moon which occurs during the penumbral phase of the eclipse could be explained if the surface material were highly insulating. They also suggested that the lack of a significant variation between their measured brightness temperature from 9-11 μ and 8-14 μ implied that the surface material must be powdered in order to reduce the high reflectivity (and hence low emissivity) that silicate minerals possess in the nine micron region. An attempt to measure the radiation during the unlit portion of lunation yielded a temperature of 120°K, although the authors noted that the observed signal was near the lower limit of their detection system.

Shorthill (1962), while observing the eclipse cooling of several bright ray craters during the 1960 eclipses of March and September with a thermistor bolometer, discovered that these craters cooled less rapidly than their surroundings. Sinton (1960) also observed the anomalous cooling of the bright ray crater Tycho during the September 1960 eclipse and suggested that the thickness of the dust layer in these bright ray craters, computed from eclipse cooling, could be used to provide relative ages. He also reported (1955) a midnight temperature of approximately 120°K for a fairly large area of the lunar disc.

In 1962, Murray and Wildey (1963a and 1963b) scanned the unilluminated Moon using a more sensitive detection and calibration system with more precise filtering (Westphal et al., 1963). Their observations indicate that differences in thermal properties exist in localities on the Moon other than in the immediate vicinity of the large bright ray craters and anomalous radiation effects persist well into the lunar nighttime. The observed lunation cooling, in areas where no significant anomalies are present, implies a midnight temperature at least 20°K colder than the lower limit of detection of Pettit and Nicholson's observations.

Theoretical models of the eclipse and lunation cooling of the Moon were first computed by Wesselink (1948). He assumed that the lunar surface was optically thick, that the emissivity was unity, and that the curvature of the Moon could be neglected since the penetration of the thermal energy is only a few centimeters. He applied the one-dimensional heat conduction equation with constant thermal properties and used Stefan's law to construct a radiation boundary condition. The resulting partial differential equations were reduced to finite difference equations

and solved by the Schmidt method. (See Appendix 6.) He concluded that the agreement between his model and Pettit's (1940) eclipse cooling observations indicates that the thermal properties of the Moon's surface layer are reasonably insensitive to temperature variations. His theoretical lunation cooling curve was computed with a thermal inertia* of 970 $cal^{-1}cm^{2}sec^{1/2}deg^{1/2}$ since this value fitted the eclipse cooling observations. The computed midnight temperature is about 20° cooler than the 120° temperature measured by Pettit and Nicholson and by Sinton, but is not inconsistent with the observations of Murray and Wildey.

A model for the thermal conductivity of powders was suggested by Wesselink in which the contact conduction of the grains was assumed negligible and the powder idealized as a series of radiating slabs. He concluded that the grain size of the powder must be less than 300 microns for radiative transfer to be negligible. Both the assumptions and conclusions of this model are at variance with the experimental investigation of selected silicate powders by the present author. The contact conduction of the powders is negligible only for the largest glass spheres with grain sizes > 300 microns and radiative transfer is significant even at the smallest grain sizes (< 40 microns).

Jaeger and Harper (1950) and Jaeger (1953a) computed the eclipse and lunation cooling for a half space (see Appendix 6) and also for a high impedance skin with negligible heat capacity overlying a half space, using the method of Laplace transforms. The assumption of constant

---

*The thermal inertia is defined equal to $(k\rho c)^{-1/2}$. (See Appendix 6.)

thermal properties was acknowledged as a simplification. Jaeger (1953a) asserted that the eclipse observations cannot be explained by a conductivity with a temperature cubed dependence.

Muncey (1958) suggested that the variation of conductivity and specific heat is proportional to temperature. Although the solution of the heat conduction equation is fairly simple with this approximation, the temperature dependence chosen is not in agreement with either the thermal conductivity measurements of this investigation or the specific heats of silicates (Birch, 1942).

## 2. THEORETICAL MODEL

The theoretical model is constructed with the same assumptions as equation 2: the thermal properties are functions only of temperature, and the emergent flux is emitted only from the surface (infinite optical thickness) and is Planckian in distribution.

$$\frac{\partial}{\partial x}\left(k(T)\,\frac{\partial T}{\partial x}\right) = \rho c(T)\,\frac{\partial T}{\partial x}$$

The surface boundary condition is

$$k\,\frac{\partial T}{\partial x}\bigg|_{x=0} = \sigma T^4\bigg|_{x=0} - h(t)$$

where $h(t)$ is the insolation (flus absorbed by the surface due to the incident solar radiation). Now define

$$\theta(T) = \int_0^T k(T)\,dT$$

The heat conduction equation reduces to

$$\frac{\partial^2\theta}{\partial x^2} = \frac{1}{\kappa}\,\frac{\partial\theta}{\partial t}$$

where

$\theta = ((x, t)$

$\kappa = \kappa(T) = \dfrac{k(T)}{\rho c(T)}$ is the thermal diffusivity

and the boundary equation becomes

$$\frac{\partial\theta}{\partial x}\bigg|_{x=0} = \sigma T^4\bigg|_{x=0} - h(t)$$

The partial differential equations are reduced to finite differences by the method of Crank and Nicholson (1947). Let

$$\theta_m^n \equiv \theta(x = m\Delta t,\ t = n\Delta t)$$

Now replacing all derivatives by first order finite differences at the mean time between two time intervals yields:

$$\frac{\partial\theta}{\partial t} = \frac{\theta_m^{n+1} - \theta_m^n}{\Delta t}$$

$$\frac{\partial^2\theta}{\partial t^2} = \frac{\theta_{m+1}^{n+1} + \theta_{m+1}^n + \theta_{m-1}^{n+1} + \theta_{m-1}^n - 2(\theta_m^n + \theta_m^{n+1})}{2\Delta x^2}$$

$$\frac{\partial\theta}{\partial x} = \frac{\theta_m^{n+1} + \theta_{m+1}^n - (\theta_{M-1}^{n+1} + \theta_{m-1}^n)}{4\Delta x}$$

$$\kappa(T) = \kappa\left(\frac{T_m^{n+1} + T_m^n}{2}\right) = \kappa_m^{n+\frac{1}{2}}$$

$$\sigma T^4\Big|_{x=0} - h(t) = \sigma(T_o^n)^3(2T_o^{n+1} - T_o^n) - \left(\frac{h^{n+1} + h^n}{2}\right)$$

Now set

$$M_m^n = \frac{\Delta t}{\Delta x^2}\kappa_m^{n+\frac{1}{2}}$$

$$\theta_o^{n+1} = \frac{M_o^n}{1+M_o^n}(\theta_1^{n+1} + \theta_1^n) + \left(\frac{1 - M_o^n}{1 + M_o^n}\right)\theta_o^n$$

$$+ \frac{2\Delta x M_o^n}{1 + M_o^n}\left[-\sigma(T_o^n)^3(2T_o^{n+1} - T_o^n) + \frac{h^{n+1} + h^n}{2}\right]$$

and for $m > 0$

$$\theta_m^{n+1} = \frac{M_m^n}{2(1 + M_m^n)} \left( \theta_{m+1}^{n+1} + \theta_{m+1}^{n} + \theta_{m-1}^{n+1} + \theta_{m-1}^{n} \right)$$

$$+ \left( \frac{1 - M_m^n}{1 + M_m^n} \right) \theta_m^n$$

These equations follow directly from the substitution of the finite differences in the differential equations and defining a fictitious level $m = -1$.

This method of solution can be examined by assuming that $T_m^n$ and hence $\theta_m^n$ are known. A guess is made of $\theta_m^{n+1}$, and the $T_m^{n+1}$ are then computed from the conductivity function. Then the values of $\theta_m^{n+1}$ are computed from the preceeding equations and this new estimate of $\theta_m^{n+1}$ replaces the original guess. The iterations proceed backward and forward in time until the iterations in each step are less than a chosen convergence value. The initial temperature distribution is chosen in the same manner as in Wesselink's solution: a guess is made of the steady state temperature at depth, and the solution is begun at a time when the insolation equals the flux emitted by the surface at this temperature.

The variation of the surface temperature for constant thermal properties indicates two important results. If the thermal inertia is greater than 100 $cal^{-1}cm^2sec^{1/2}deg^{1/2}$ then the surface temperature during the daytime portion of lunation is controlled by the surface reflectivity, while the surface temperature during the nightime portion is controlled by the thermal inertia (figs. 8 and 9). The region of the morning and evening terminators involves a combination of the effects

FIGURE EIGHT

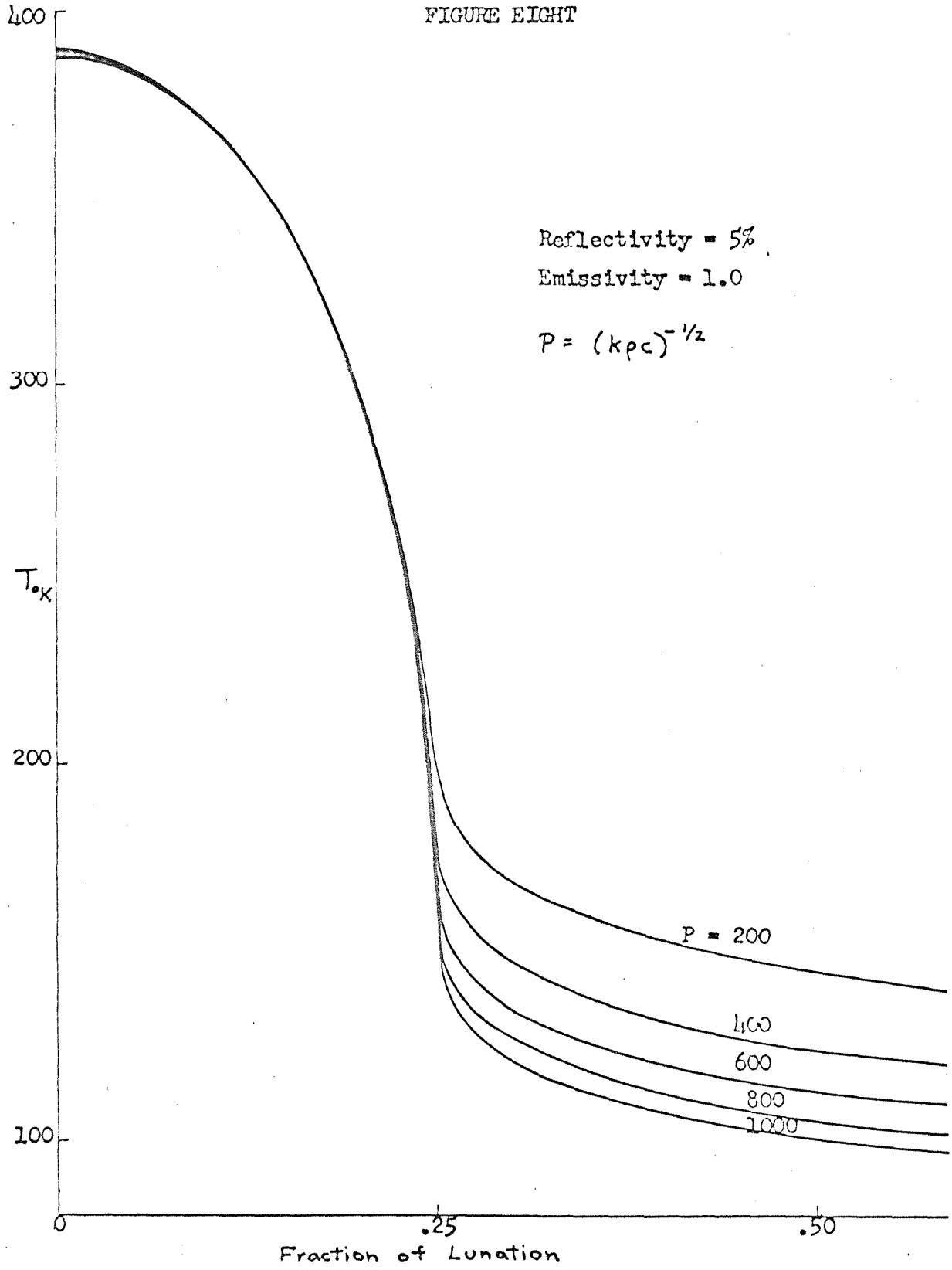


Lunation Surface Temperature As A Function of P, The Thermal Inertia

FIGURE NINE

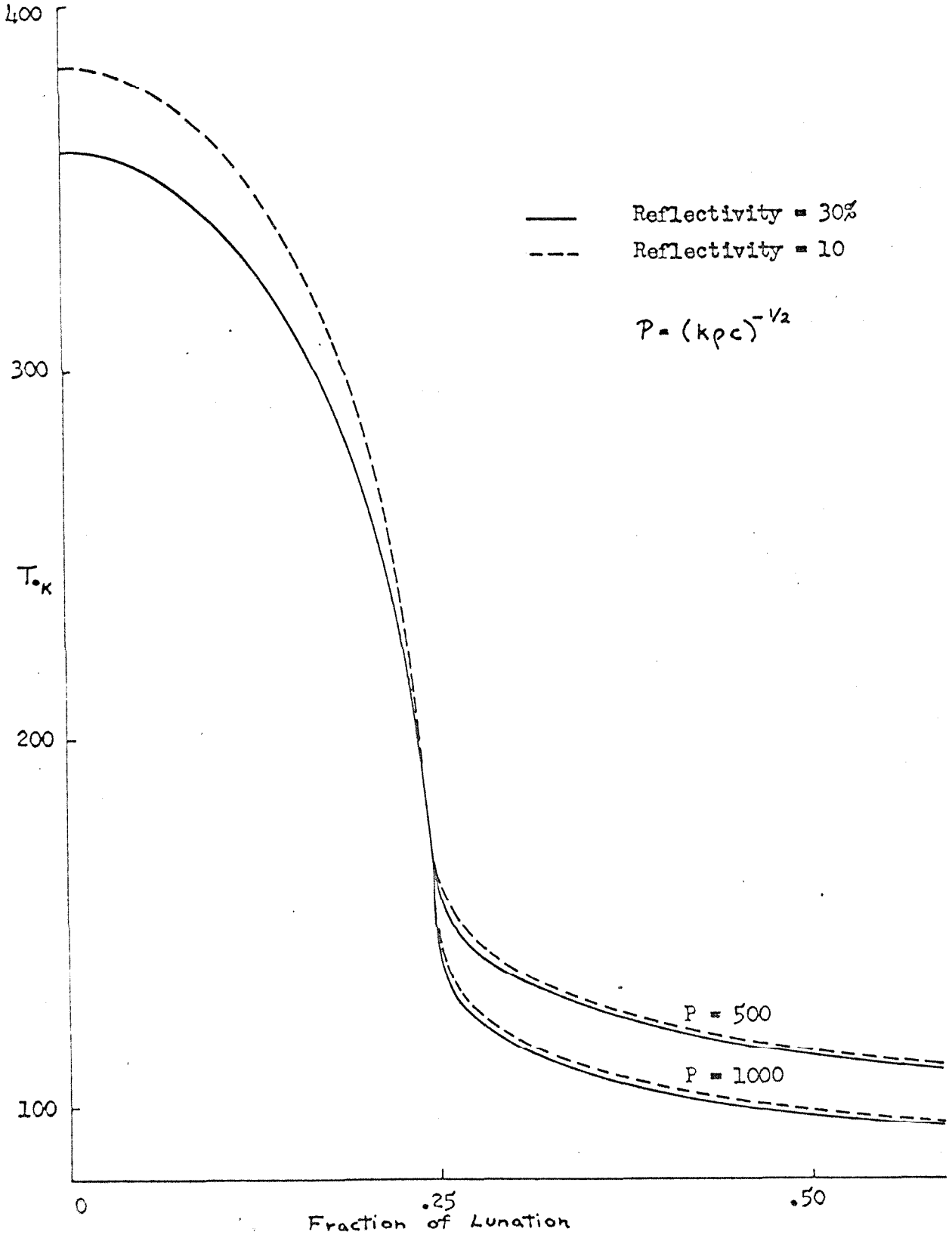


Surface Temperature During Lunation Cooling As A Function of Thermal Inertia and Reflectivity

due to reflectivity and thermal properties. It is this dependence of the surface temperature on the reflectivity during the illuminated phase which implies that the choice of the initial temperature distribution can be fairly arbitrary, provided that the temperature at depth is in reasonable agreement with the mean surface temperature. This surface temperature variation also suggests that the transient solution derived from the initial temperature distribution during the first period of the heating and cooling cycle will not be significantly different from the steady state periodic solution. The agreement between the surface temperatures computed from the numerical solution outlined, assuming constant thermal properties, and Jaeger's exact periodic solution for constant thermal properties seems to justify the assumption that these equations can be used to describe adequately the assumed model.

# 3. COMPARISON OF THEORETICAL MODELS WITH LUNATION COOLING

The observed lunation cooling (Murray and Wildey, 1963b) was obtained by scanning across the Moon's apparent disc in right ascension. The scan number 1 (August 21-22, 1963) is nearly an equatorial scan and for this reason will be used to compare with the theoretical cooling curves. The similarity between this scan and several other scans across the Moon indicates that it is probably representative of the average lunation cooling. Although the general practice in comparing eclipse cooling observations with theoretical models is to reduce the observations to surface temperatures and plot directly on the computed cooling curve, it was felt that a more accurate comparison could be obtained in the following manner. Theoretical cooling curves were computed and reduced to signal deflections using the Planck function and the response curve of the detector multiplied by the atmospheric extinction. The time scale of the theoretical cooling curves was then related to the recording time scale of the observations by mapping the angular scan rate onto the surface of the Moon.

This method of comparison between the observed signal and the theoretical model has two significant advantages: it permits a direct examination of the possibility of lateral variation within the photometer resolution (since the signals are additive), and it provides a more meaningful examination at the lower temperatures where signal fluctuations are significant.

Figure 10 is a comparison between the observed signal and the

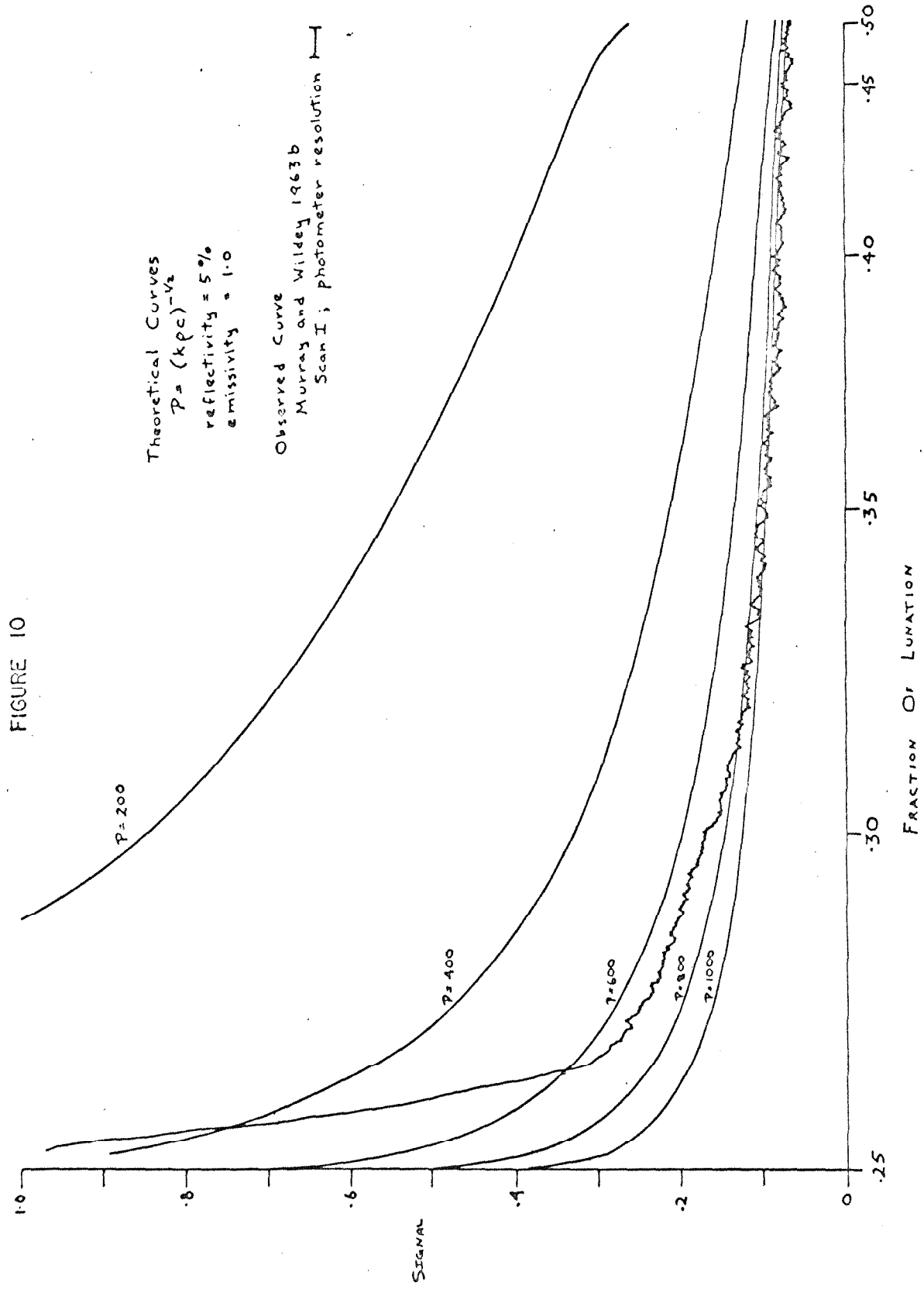
Theoretical Curves
P = (kρc)^-½
reflectivity = 5%
emissivity = 1.0
Observed Curve
Murray and Wildey 1963b
Scan I; photometer resolution
P=200
P=400
P=600
P=800
P=1000
SIGNAL
1.0
.8
.6
.4
.2
0
.25
.30
.35
.40
.45
.50
FRACTION OF LUNATION

FIGURE 10

theoretical signals computed for constant thermal property models. It is clear that the lunation observations are not compatible with a homogeneous model with constant thermal properties. The observed cooling curves might be interpreted as indicating that the thermal properties of the lunar surface decrease with decreasing temperature.

To examine this possibility theoretical cooling curves were computed using the experimental conductivities obtained in the first section of this investigation. The specific heats of several silicates (Birch, 1942), as a function of temperature, are plotted in fig. 11. A least squares quadratic fit to the quartz and quartz glass data is indicated by the dashed line.

The curves 3, 4, 5, 6 in fig. 12 were computed for homogeneous models composed of silica glass spheres of various grain sizes: the conductivities used are those derived from the first order theory in Part I, the specific heats are based on the quadratic fit to Birch's data, and a density of 1.5 gm/cm$^3$ was chosen. Although these theoretical cooling curves are steeper than the constant thermal property cooling curves, the temperatures in the region of the evening terminator are clearly too low. Two other cooling curves (1 and 2) were computed with a contact conduction of 500 ergs/cm/sec/deg, a density of 1.5 gm/cm$^3$, and bulk opacities of 100 and 10 cm$^{-1}$. These models provide a significant improvement in matching the observed evening terminator temperature but their temperatures are somewhat too high during the remainder of the unilluminated portion of lunation. Reducing the density of these fictitious models reduces their terminator temperatures and flattens out the cooling curve.

FIGURE ELEVEN

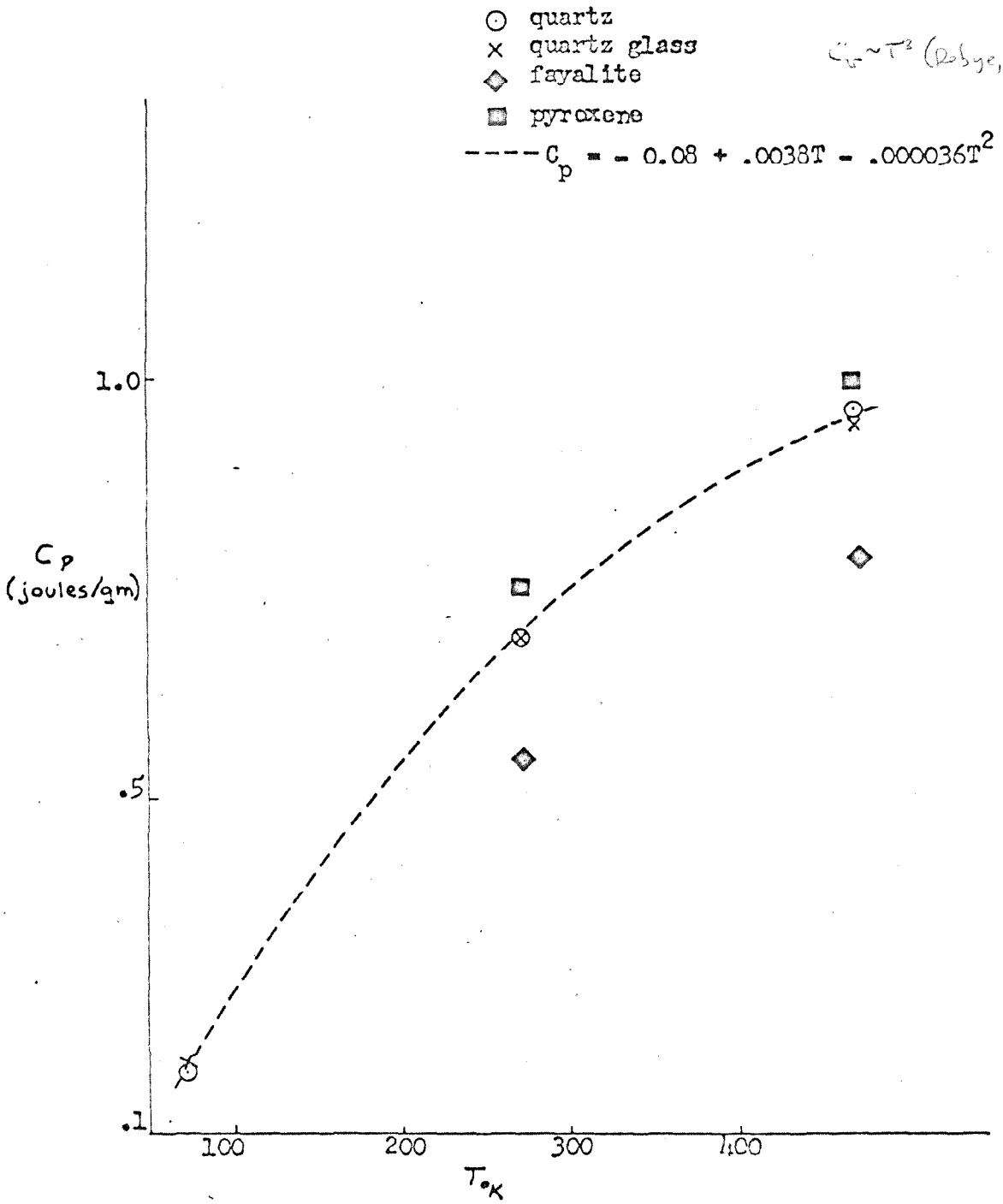


Specific Heat As A Function of Temperature for Several Silicates

FIGURE 12

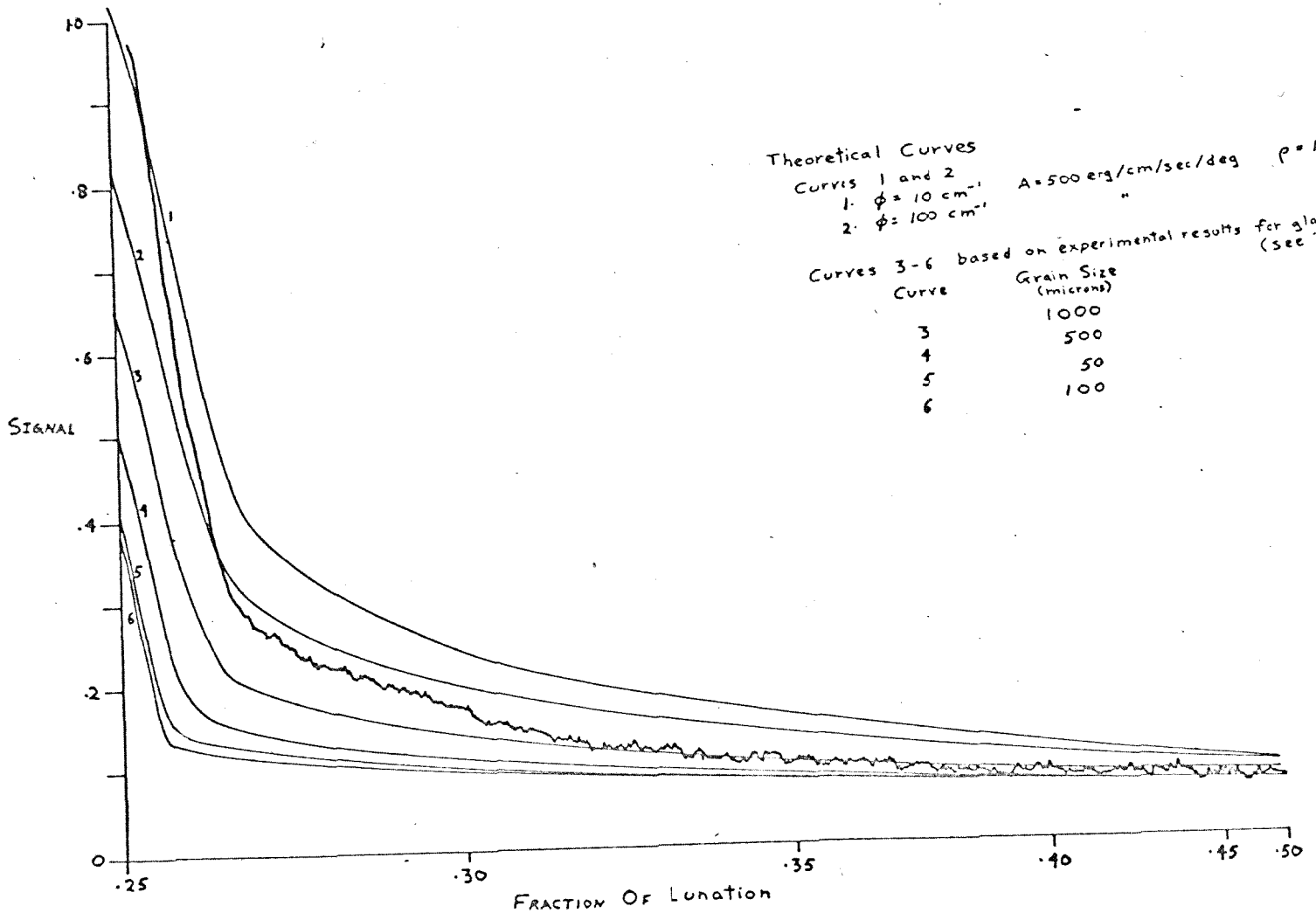


Theoretical Curves

Curves 1 and 2

1. $\phi$ = 10 cm$^{-1}$ A = 500 erg/cm/sec/deg $\rho$ = 1.5 gm/cm$^3$
2. $\phi$ = 100 cm$^{-1}$ "

Curves 3-6 based on experimental results for glass spheres (see Text 3.0)

| Curve | Grain Size (microns) |
|---|---|
| 3 | 1000 |
| 4 | 500 |
| 5 | 50 |
| 6 | 100 |

It seems unlikely that any reasonable physical model for the lunar surface can be constructed which is homogeneous to a depth of several centimeters and extends over an area of a few tens of kilometers (the photometer resolution was 50 kms. near the terminator in Murray's and Wildey's observations).

It is recalled that the eclipse cooling observations of Pettit and Nicholson were adequately described by a homogeneous model with a thermal inertia of 1000 $cal^{-1}cm^{2}sec^{1/2}deg^{1/2}$. The short cooling times during the eclipse imply that these observations are dependent on the thermal properties only of the upper few millimeters of the lunar surface. Jaeger's (1953) analysis of the cooling of a thin surface layer overlying a more conductive homogeneous semi-infinite slab with constant thermal properties indicates that the most significant effect of the layering is to reduce the cooling rate compared with the cooling of a semi-infinite slab which has the same thermal properties as the layer.

The large evening terminator temperatures and rapid cooling during the initial portion of nighttime lunation does not seem to be compatible with a simple layering model. It is suggested that the effects of layering can best be examined in the region of the morning terminator since the surface has cooled for fourteen days.

# 4. CONCLUSIONS

The eclipse observations of Pettit and Nicholson seem to be reasonably explained by theoretical models with constant thermal properties which are independent of depth and lateral variation. The recent lunation observations of Murray and Wildey are not in agreement with this simple model. Theoretical models based on experimental measurements of the thermal conductivity of selected silicate powders in vacuum, existing specific heat data, and the assumption of homogeneous thermal properties do not provide an adequate explanation of these observations. It is concluded that no simple model of the thermal properties of the lunar surface can be derived at present which is consistent with the eclipse observations of Pettit and Nicholson and the recent lunation observations of Murray and Wildey.

# REFERENCES

Aberdeen, J., and T. H. Laby, 1926, Proceedings of the Royal Society, vol. 113, pp. 459-477.

Birch, F., 1942, Special Paper 36, Geological Society of America, pp. 223-266.

Burns, E. A., and R. Lyon, 1963, presented at the Lunar Surface Materials Conference, Boston, Mass.

Cline, D., and R. H. Kropschot, 1963, in Radiative Transfer from Solid Materials, ed. Blau and Fischer (Macmillan), p. 61.

Chandrasekhar, S., 1960, Radiative Transfer (New York: Dover Publications).

Crank, J., and P. Nicholson, 1947, Proceedings of the Cambridge Philosophical Society, vol. 43, pp. 50-67.

Dana, E. S., 1955, Dana's Manual of Mineralogy, 16th edition, revised C. S. Hurlbut Jr. (New York: Wiley and Sons), p. 314.

Hertz, H., 1895, Miscellaneous Papers (London, Macmillan).

Jaeger, J. C., and A. F. A. Harper, 1950, Nature, vol. 166, p. 1026.

_____, 1953a, Australian Journal of Physics, vol. 6, pp. 10-21.

_____, 1953b, Cambridge Philosophical Society Proceedings, vol. 49, pp. 355-359.

Jakob, M., 1949, Heat Transfer (New York: Wiley and Sons).

Kannuluik, W. G., and L. H. Martin, 1933, Proceedings of the Royal Society, A141, pp. 144-157.

Langley, S. P., 1887, Memoirs of the National Academy of Sciences, vol. 4, p. 107.

Launer, P., 1952, American Minerologist, vol. 37, pp. 764-784.

Muncey, R. W., 1958, Nature, vol. 181, pp. 1458-1459.

Münch, G., 1960, in Stellar Atmospheres, ed. J. L. Greenstein (Chicago: University of Chicago Press), pp. 1-49.

Murray, B. C., and R. L. Wildey, 1963a, Astrophysical Journal, vol. 137, p. 692.

_____, 1963b, Astrophysical Journal, in press.

Pettit, E., and S. B. Nicholson, 1930, Astrophysical Journal, vol. 71, pp. 102-135.

_____, 1940, Astrophysical Journal, vol. 91, pp. 408-420.

Roddy, D. T., Rittenhouse, J. B., and R. F. Scott, American Institute of Aeronautics and Astronautics Journal, vol. 1, pp. 868-873.

Rosse, Lord, 1869, Proceedings of the Royal Society, vol. 17, p. 436.

Shorthill, R. W., 1962, Boeing Document D1-82-0196, presented at the Conference on Lunar Exploration held at Virginia Polytechnic Institute, August 13-17.

Sinton, W. M., 1960, Lowell Observatory Bulletin, No. 108, Vol. 5.

_____, 1955, Journal of Optical Society of America, vol. 45, pp. 975-979.

Smoluchowski, M., 1910, Krakauer Anzeiger (A), p. 129.

Watson, K., and C. A. Bauman, 1963, Review of Scientific Instruments (to be published in vol. 11)

Wesselink, A. J., 1948, Bulletin of the Astronomical Institutes of the Netherlands, vol. 10, pp. 351-363.

Westphal, J. A., Murray, B. C. and D. E. Martz, 1963, Applied Optics, vol. 2, pp. 749-753.

Woolley, R. v. d. R., and D. W. N. Stibbs, 1953, The Outer Layers of a Star (London: Clarendon Press).

## Appendix 1

## SAMPLE PREPARATION AND DESCRIPTION

The glass spheres (a soda-lime-silica glass) were obtained commercially from Microbeads Inc., Jackson, Miss. The spheres were described as 95% true spheres with less than 2% of the particles exceeding the maximum grain size and less than 8% of the particles smaller than the minimum grain size. As a check the 53-74 μ spheres were sieved through a 270 U. S. Standard Sieve (53 μ). No appreciable amount of sample passed through the sieve during the processing of several hundred grams of sample for many hours on the Rotap sieve shaker. It was concluded that the stated grain size range is probably quite accurate. The samples were also examined under the microscope during the thickness measurements. Although a few per cent of the grains tended to be nonspherical there were no angular fragments observed for grain sizes greater than 40 μ. The solid glass (as opposed to the beads in bulk) was stated to have a density of 2.5 $gm/cm^3$, a thermal conductivity of $1.05 \times 10^5$ ergs/cm/sec/deg and a modulus of elasticity of $7.6 \times 10^{11}$ $dynes/cm^2$.

The crushed glass spheres were prepared by taking about 500 grams of the largest spheres (840 - 590 μ) and crushing them in the ceramic ball mill in 50 gram portions for about one half hour. The crushed fragments were then sieved between 74 and 44 μ on the Rotap sieve shaker.

The quartz sample was from a Pre Cambrian pegmatite at Wickenburg, Arizona. The uncrushed slab was free of inclusions

either in the form of air bubbles or impurities. The olivine was from a dunite at Webster, North Carolina, and the amphibole was a pegmatite hornblende from the San Gabriel Mountains, California.

The quartz was crushed and sieved in two grain size ranges, 44 - 74 μ and less than 74 μ. The hornblende and the olivine were both crushed and sieved less than 74 μ. The small weights of the hornblende and olivine samples prevented a selection of a 44 - 77 μ fraction, since the thermal conductivity measurements generally required a sample weight in excess of 40 grams.

Some contamination of the crushed samples resulted from the crushing in the ceramic ball mill with the ceramic balls. The samples were acid washed and dried in an evaporating acetone solution to remove as much of the absorbed water as possible.

## Appendix 2

## RADIATIVE TRANSFER

The treatment and formulation of the basic equations for radiative transfer are discussed in studies of stellar atmospheres, e.g., Wooley and Stibbs (1953), Münch (1960), and Chandrasekhar (1960).

The solution of the equation of transfer in a homogeneous semi-infinite body in a state of radiative equilibrium and in local thermodynamic equilibrium reduces to a simple form when the absorption coefficient is independent of wavelength.

$$T^4(\tau) = \frac{3\pi F}{4\sigma} [\tau + q(\tau)]$$

where

$\tau$ is the optical depth

$\pi F$ is the net integrated flux

$\sigma$ is the Stefan Boltzmann constant

$T = T(\tau)$ is the temperature

and $q(\tau)$ is a monotonic increasing function of $\tau$ and bounded:

$$\frac{1}{\sqrt{3}} \leq q(\tau) < 0.711$$

Since $dz = - d\tau/\bar{k}\rho$ where $z$ is the reference axis into the half space, $\bar{k}$ is the mass absorption coefficient and $\rho$ is the density, then

$$- \frac{16\sigma T^3}{3\bar{k}\rho} \frac{dT}{dz} = \pi F$$

since $dq/d\tau$ is negligible for $\tau > 0$.

An effective radiative conductivity can be defined:

$$- K_e \frac{dT}{dz} = \pi F$$

hence

$$K_e = \frac{16\sigma T^3}{3\bar{k}\rho}$$

If the absorption coefficient is not independent of frequency then the optical thickness is undefined. For $\tau >> 1$ the Roseland mean can be used:

$$\frac{1}{\bar{k}_R} \int_o^\infty \frac{dB_\nu}{dT} d\nu = \int_o^\infty \frac{1}{k_\nu} \frac{dB_\nu}{dT} d\nu$$

where $B_\nu$ is the Planck function and $\nu$ the frequency.

We have ignored scattering in our treatment of radiative transfer. If the scattering is isotropic and the absorption and emission take place under local thermodynamic equilibrium then

$$S_\nu = \frac{k_\nu}{k_\nu + \sigma_\nu} B_\nu + \frac{k_\nu}{k_\nu + \sigma_\nu} J_\nu$$

where $S_\nu$ is the source function, $J_\nu$ the mean intensity and $k_\nu$ and $\sigma_\nu$ the mass absorption and scattering coefficients.

At large optical depths $B_\nu \sim J_\nu$, hence $S_\nu = B_\nu$ as in the pure absorption case. The mean optical thickness $\tau$ is then defined by

$$\tau = \int_z^o (\bar{k} + \bar{s}) \rho \, dz$$

where $\bar{k}$ and $\bar{s}$ are mean absorption and scattering coefficients.

It is clear that for $\tau$ large the absorption and scattering processes can be treated as pure absorption provided that the scattering

is isotropic.

The mass absorption coefficients computed from the experimental results of the author's conductivity measurements indicate that $\tau = 1$ at a depth less than a single grain. This will be considered as a sufficient justification for assuming that the radiative transfer can be adequately described by the treatment presented in this Appendix.

## Appendix 3

## EMISSIVITY EFFECTS

It was assumed in the derivation of equation 2 that the brightness, effective, and kinetic surface temperatures are equal. This assumption will now be investigated for the optically thick case.

Define $\bar{\epsilon}(T)$ the effective mean emissivity and $\bar{\bar{\epsilon}}(T)$ an effective 8-14 micron emissivity as follows:

$$\bar{\epsilon}(T) = \frac{\int_0^\infty F(\lambda, T)\epsilon(\lambda)\, d\lambda}{\int_0^\infty F(\lambda, T)\, d\lambda}$$

and

$$\bar{\bar{\epsilon}}(T) = \frac{\int_8^{14} F(\lambda, T)r(\lambda)\epsilon(\lambda)\, d\lambda}{\int_8^{14} F(\lambda, T)r(\lambda)\, d\lambda}$$

where

$F(\lambda, T)$ is the Planck function

$\epsilon(\lambda)$ is the emissivity of the sample surface from $\lambda$ to $\lambda + d\lambda$

$r(\lambda)$ is the response of the detector

Let $T_L$, $\bar{\bar{T}}_L$, and $\bar{T}_L$ be the kinetic surface temperature, the brightness and the effective temperature.

Now expressing equation 5 in the exact form (but assuming infinite optical thickness)

$$\int_{T_L}^{T_B} K(T)\, dT = \sigma(\bar{\bar{T}}_L^4 - T_W^4) \cdot L$$

where $\overline{\overline{T}}_L$ the brightness temperature is computed from the detector signal.

Now $S(\overline{T}_L) = \overline{\overline{\epsilon}}(\overline{T}_L)S(T_L)$ where $S = S(T)$ is the response function of the detector.

It will be shown that the variations of $\overline{\overline{\epsilon}}$ with temperature are insignificant over the range of sample surface temperatures that are measured in this experimental investigation.

$$\overline{\overline{\epsilon}}(\overline{T}_L) \sim \overline{\overline{\epsilon}}_{mean}$$

The effective temperature and the kinetic temperature are related by

$$\overline{\epsilon}(T_L)\sigma T_L^4 = \sigma \overline{\overline{T}}_L^4$$

By a similar argument

$$\overline{\epsilon}(T_L) \sim \overline{\epsilon}_{mean}$$

Burns and Lyons (1963) have measured the emissivity of quartz and quartz sand as a function of wavelength from 5 μ to 30 μ. $\overline{\epsilon}$ and $\overline{\overline{\epsilon}}$ were numerically computed with their results assuming that the emissivities were unity for wavelengths greater than 30 μ. Their data suggest that this approximation is probably valid in the vicinity of 30 μ.

| Temperature | Quartz Plate | | 400 μ Quartz Sand | | 40 μ Quartz Sand | |
|---|---|---|---|---|---|---|
| °K | $\overline{\epsilon}$ | $\overline{\overline{\epsilon}}$ | $\overline{\epsilon}$ | $\overline{\overline{\epsilon}}$ | $\overline{\epsilon}$ | $\overline{\overline{\epsilon}}$ |
| 100 | 0.93 | 0.80 | 0.98 | 0.90 | 0.98 | 0.91 |
| 150 | 0.86 | 0.74 | 0.95 | 0.88 | 0.96 | 0.89 |
| 200 | 0.81 | 0.70 | 0.93 | 0.86 | 0.94 | 0.88 |
| 250 | 0.80 | 0.68 | 0.92 | 0.85 | 0.93 | 0.87 |

The experimental results were rerun using $\overline{\epsilon} = 0.95$ and $\overline{\overline{\epsilon}} = 0.88$, since the majority of surface temperatures were less than 200°K. The changes in A and B using these emissivities are small in comparison with the experimental errors. (See Appendix 4, Part 3.)

Appendix 4

# EXPERIMENTAL RESULTS

## Part 1

The experimental results are tabulated for the various samples. Only the final steady state signals are given. A list of abbreviations used in the table are given below:

| | |
|---|---|
| MICRO 203 | glass spheres, 840 - 590 μ |
| " 456 | " 350 - 250 μ |
| " 1217 | " 125 - 88 μ |
| " 2027 | " 74 - 53 μ |
| " 4000 | " < 37 μ |
| CRD BEADS | crushed glass spheres 74 - 44 μ |
| CRD QTZ | crushed quartz 74 - 44 μ |
| CRD QTZ* | " " < 74 μ |
| CRD HRNB* | " hornblende < 74 μ |
| CRD HRNB*$ | " " " |
| CRD OLV*$ | " olivine < 74 μ |

Note: $ used to indicate samples which were contained in a leucite cylinder to provide a thicker sample.

APPENDIX TWO

| SAMPLE | WEIGHT GMS. | CENTER THICKNESS GMS. | MEAN THICKNESS CMS. | BATH TEMP DEG. K | CALIB. TEMP SEG. K | SAMPLE SIGNAL M.V. | CALIB. SIGNAL M.V. |
|---|---|---|---|---|---|---|---|
| MICRO 203 | 298.3 | 0.78 | 0.66 | 279.9 | 295.0 | 33. | 1050. |
| | | | | 296.2 | 295.8 | 61. | 1280. |
| | | | | 319.0 | 299.8 | 82. | 1078. |
| MICRO 203 | 136.4 | 0.47 | 0.31 | 319.9 | 297.9 | 161. | 1050. |
| | | | | 295.5 | 294.8 | 79. | 850. |
| | | | | 280.1 | 293.6 | 52. | 850. |
| MICRO 203 | 135.9 | 0.41 | 0.34 | 279.4 | 294.1 | 75. | 1103. |
| | | | | 296.2 | 295.2 | 118. | 1120. |
| | | | | 321.6 | 299.0 | 275. | 1500. |
| MICRO 203 | 79.0 | 0.20 | 0.20 | 295.7 | 298.7 | 407. | 1980. |
| | | | | 336.9 | 301.7 | 990. | 2445. |
| | | | | 276.1 | 295.7 | 315. | 2305. |
| MICRO 203 | 318.9 | 0.90 | 0.78 | 297.1 | 300.1 | 94. | 1030. |
| | | | | 337.1 | 302.7 | 91. | 980. |
| | | | | 277.5 | 297.0 | 84. | 1925. |
| MICRO 456 | 119.0 | 0.34 | 0.32 | 296.6 | 298.9 | 138. | 2330. |
| | | | | 279.0 | 296.2 | 92. | 2355. |
| | | | | 332.5 | 301.2 | 301. | 2540. |
| MICRO 456 | 172.6 | 0.50 | 0.43 | 296.5 | 299.4 | 85. | 2770. |
| | | | | 346.6 | 303.5 | 232. | 2810. |
| | | | | 277.5 | 296.8 | 48. | 2550. |
| MICRO 1217 | 129.4 | 0.40 | 0.32 | 295.2 | 294.6 | 34. | 1047. |
| | | | | 322.7 | 298.3 | 62. | 1140. |
| | | | | 280.4 | 294.4 | 24. | 1015. |
| MICRO 1217 | 128.7 | 0.41 | 0.33 | 279.3 | 293.6 | 27. | 1525. |
| | | | | 294.4 | 293.7 | 29. | 1150. |
| | | | | 318.7 | 298.3 | 71. | 1660. |
| MICRO 2027 | 75.3 | 0.20 | 0.18 | 296.3 | 299.3 | 109. | 2060. |
| | | | | 333.4 | 302.5 | 244. | 2465. |
| | | | | 277.5 | 296.6 | 98. | 2440. |

APPENDIX 1.0

| SAMPLE | WEIGHT GMS. | CENTER THICKNESS GMS. | MEAN THICKNESS CMS. | BATH TEMP DEG. K | CALIB. TEMP DEG. K | SIGNAL N.V. | CALIB. SIGNAL N.V. |
|---|---|---|---|---|---|---|---|
| MICRO 2027 | 86.0 | 0.20 | 0.25 | 297.3 | 299.8 | 87. | 1910. |
| | | | | 346.1 | 303.1 | 220. | 2330. |
| | | | | 277.2 | 296.1 | 72. | 2210. |
| MICRO 2027 | 147.1 | 0.40 | 0.37 | 296.2 | 299.6 | 43. | 1700. |
| | | | | 343.1 | 303.6 | 101. | 2200. |
| | | | | 277.1 | 297.7 | 36. | 1910. |
| MICRO 4000 | 102.1 | 0.29 | 0.32 | 318.6 | 297.2 | 102. | 1149. |
| | | | | 295.0 | 294.7 | 69. | 1075. |
| | | | | 279.3 | 293.8 | 70. | 1405. |
| MICRO 4000 | 234.0 | 0.80 | 0.64 | 327.1 | 299.3 | 51. | 1775. |
| | | | | 281.0 | 294.0 | 28. | 2550. |
| | | | | 295.0 | 294.0 | 38. | 2490. |
| MICRO 4000 | 93.6 | 0.43 | 0.27 | 328.1 | 299.1 | 169. | 3120. |
| | | | | 280.9 | 293.3 | 51. | 2000. |
| | | | | 295.3 | 294.7 | 75. | 2250. |
| MICRO 4000 | 102.1 | 0.40 | 0.35 | 279.6 | 293.7 | 39. | 1300. |
| | | | | 295.9 | 295.0 | 68. | 1685. |
| | | | | 320.8 | 297.5 | 99. | 1675. |
| CRD BEADS | 57.1 | 0.42 | 0.32 | 296.3 | 298.8 | 90. | 1750. |
| | | | | 332.6 | 301.7 | 180. | 2225. |
| | | | | 276.5 | 296.9 | 81. | 2120. |
| CRD BEADS | 50.3 | 0.34 | 0.35 | 296.3 | 299.8 | 110. | 2135. |
| | | | | 343.0 | 302.9 | 250. | 2550. |
| | | | | 276.4 | 296.2 | 92. | 2260. |
| CRD BEADS | 51.3 | 0.28 | 0.24 | 295.7 | 298.9 | 197. | 2200. |
| | | | | 341.6 | 303.0 | 410. | 2575. |
| | | | | 276.5 | 296.3 | 150. | 2250. |
| CRD QTZ | 79.0 | 0.35 | 0.26 | 316.8 | 297.9 | 338. | 2350. |
| | | | | 295.5 | 295.0 | 236. | 2090. |
| | | | | 280.5 | 293.2 | 170. | 1885. |
| CRD QTZ | 163.6 | 0.54 | 0.45 | 340.0 | 301.8 | 380. | 2785. |
| | | | | 276.9 | 294.1 | 197. | 2980. |
| | | | | 295.1 | 294.4 | 249. | 3000. |

APPENDIX TWO

| SAMPLE | WEIGHT GMS. | CENTER THICKNESS GMS. | MEAN THICKNESS CMS. | BATH TEMP DEG. K | CALIB. TEMP SEG. K | SAMPLE SIGNAL M.V. | CALIB. SIGNAL M.V. |
|---|---|---|---|---|---|---|---|
| CRD QTZ* | 30.9 | 0.40 | 0.42 | 296.3 | 299.5 | 215. | 1860. |
| | | | | 344.5 | 303.1 | 500. | 2270. |
| | | | | 276.7 | 296.1 | 187. | 2075. |
| CRD QTZ* | 41.2 | 0.20 | 0.15 | 297.1 | 299.6 | 236. | 1660. |
| | | | | 345.5 | 303.5 | 554. | 2170. |
| | | | | 279.8 | 296.6 | 239. | 2025. |
| CRD HRNB*$ | 46.4 | 0.60 | 0.52 | 296.0 | 299.5 | 96. | 1540. |
| | | | | 344.6 | 303.0 | 222. | 1880. |
| | | | | 277.3 | 296.8 | 74. | 1750. |
| CRD HRNB* | 47.0 | 0.20 | 0.15 | 297.0 | 298.9 | 114. | 1800. |
| | | | | 340.6 | 302.3 | 272. | 2250. |
| | | | | 277.7 | 296.8 | 98. | 2100. |
| CRD OLV+$ | 29.3 | 0.41 | 0.36 | 295.9 | 298.8 | 110. | 1610. |
| | | | | 342.9 | 302.7 | 299. | 1950. |
| | | | | 278.2 | 296.3 | 90. | 1820. |
| CRD OLV+$ | 29.3 | 0.42 | 0.36 | 278.3 | 298.8 | 95. | 1510. |
| | | | | 294.8 | 302.5 | 220. | 1869. |
| | | | | 343.1 | 296.2 | 73. | 1738. |

Part 2

The experimental results are computed as described in Section 6. The units are: B in ergs/cm/sec/deg and A in ergs/cm/sec/deg$^4$. The errors which are indicated by the +/- are computed from the standard deviation. A second set of errors are computed for B and A due to the standard deviation of the mean value of B/A. The expressions, mean and brightness emissivity, refer to the mean and effictive 8 - 14 $\mu$ emissivities computed in Appendix 3.

UNCRUSHED MICROBEADS 840-590M

BRIGHTNESS EMISSIVITY = 1.00
MEAN EMISSIVITY = 1.00

| THICKNESS CMS | DENSITY $G/CMS^3$ | BATH TEMP | KINETIC TEMP | BRIGHTNESS TEMP | EFFECTIVE TEMP | A | B |
|---|---|---|---|---|---|---|---|
| 0.78 | 1.82 | 279.9 | 171.65 | 171.65 | 171.65 | 0.000028357 | -7.1 |
| | | 296.2 | 181.51 | 181.51 | 181.51 | 0.000028446 | -7.1 |
| | | 319.0 | 194.12 | 194.12 | 194.12 | 0.000027701 | -6.9 |
| 0.47 | 1.77 | 319.9 | 213.74 | 213.74 | 213.74 | 0.000026353 | -6.6 |
| | | 295.5 | 197.69 | 197.69 | 197.69 | 0.000026420 | -6.6 |
| | | 280.1 | 186.39 | 186.39 | 186.39 | 0.000025608 | -6.4 |
| 0.41 | 1.61 | 279.4 | 188.97 | 188.97 | 188.97 | 0.000024281 | -6.0 |
| | | 296.2 | 200.97 | 200.97 | 200.97 | 0.000024773 | -6.2 |
| | | 321.6 | 220.30 | 220.30 | 220.30 | 0.000026122 | -6.5 |
| 0.20 | 1.59 | 295.7 | 226.23 | 226.23 | 226.23 | 0.000023603 | -5.9 |
| | | 336.9 | 256.25 | 256.25 | 256.25 | 0.000022821 | -5.7 |
| | | 276.1 | 211.17 | 211.17 | 211.17 | 0.000023514 | -5.9 |
| 0.90 | 1.64 | 297.1 | 180.89 | 180.89 | 180.89 | 0.000031836 | -7.9 |
| | | 337.1 | 198.95 | 198.95 | 198.95 | 0.000027798 | -6.9 |
| | | 277.5 | 169.21 | 169.21 | 169.21 | 0.000031792 | -7.9 |

$(B/A)_{MEAN}$ = -248904. +/- 2100480.

A = 0.000026628 +/- 0.000002749 +/- 0.000003628

B = -6.6 +/- 0.7 +/- 55.0

MEAN ABSORPTION COEFFICIENT = 11.36 +/- 1.55

UNCRUSHED MICROBEADS 350-250M

BRIGHTNESS EMISSIVITY = 1.00
MEAN EMISSIVITY = 1.00

| THICKNESS CMS | DENSITY G/CMS$^3$ | BATH TEMP | KINETIC TEMP | BRIGHTNESS TEMP | EFFECTIVE TEMP | A | B |
|---|---|---|---|---|---|---|---|
| 0.34 | 1.50 | 296.6 | 187.40 | 187.40 | 187.40 | 0.000013493 | 9.6 |
| | | 279.0 | 177.04 | 177.04 | 177.04 | 0.000013530 | 9.6 |
| | | 332.5 | 209.50 | 209.50 | 209.50 | 0.000013664 | 9.7 |
| 0.50 | 1.61 | 296.5 | 172.86 | 172.86 | 172.86 | 0.000013448 | 9.5 |
| | | 346.6 | 197.91 | 197.91 | 197.91 | 0.000012718 | 9.0 |
| | | 277.5 | 162.42 | 162.42 | 162.42 | 0.000013359 | 9.5 |

(B/A) = 708576. +/- 687497.
MEAN

A = 0.000013366 +/- 0.000000328 +/- 0.000000581

B = 9.5 +/- 0.2 +/- 9.6

MEAN ABSORPTION COEFICIENT = 22.63 +/- 0.99

UNCRUSHED MICROBEADS 125-88 M

BRIGHTNESS EMISSIVITY = 1.00
MEAN EMISSIVITY = 1.00

| THICKNESS CMS | DENSITY $G/CMS^3$ | BATH TEMP | KINETIC TEMP | BRIGHTNESS TEMP | EFFECTIVE TEMP | A | B |
|---|---|---|---|---|---|---|---|
| 0.40 | 1.63 | 295.2 | 172.50 | 172.50 | 172.50 | 0.000008948 | 33.9 |
| | | 322.7 | 185.36 | 185.36 | 185.36 | 0.000008807 | 33.3 |
| | | 280.4 | 165.76 | 165.76 | 165.76 | 0.000009045 | 34.2 |
| 0.41 | 1.57 | 279.3 | 160.53 | 160.53 | 160.53 | 0.000008024 | 30.4 |
| | | 294.4 | 167.35 | 167.35 | 167.35 | 0.000007994 | 30.3 |
| | | 318.7 | 179.78 | 179.78 | 179.78 | 0.000008203 | 31.1 |

(B/A) MEAN = 3783838. +/- 2508457.

A = 0.000008501 +/- 0.000000477 +/- 0.000001207

B = 32.2 +/- 1.8 +/- 25.9

MEAN ABSORPTION COEFICIENT = 35.57 +/- 5.08

UNCRUSHED MICROBEADS 74-53 M

BRIGHTNESS EMISSIVITY = 1.00
MEAN EMISSIVITY = 1.00

| THICKNESS CMS | DENSITY $G/CMS^3$ | BATH TEMP | KINETIC TEMP | BRIGHTNESS TEMP | EFFECTIVE TEMP | A | B |
|---|---|---|---|---|---|---|---|
| 0.20 | 1.68 | 296.3 | 185.43 | 185.43 | 185.43 | 0.000003330 | 67.7 |
| | | 333.4 | 202.66 | 202.66 | 202.66 | 0.000003502 | 71.3 |
| | | 277.5 | 177.52 | 177.52 | 177.52 | 0.000003301 | 67.2 |
| 0.20 | 1.38 | 297.3 | 181.80 | 181.80 | 181.80 | 0.000002958 | 60.2 |
| | | 346.1 | 201.65 | 201.65 | 201.65 | 0.000002988 | 60.9 |
| | | 277.2 | 172.91 | 172.91 | 172.91 | 0.000002868 | 58.3 |
| 0.40 | 1.60 | 296.2 | 169.03 | 169.03 | 169.03 | 0.000004083 | 83.1 |
| | | 343.1 | 183.06 | 183.06 | 183.06 | 0.000003815 | 77.5 |
| | | 277.1 | 162.75 | 162.75 | 162.75 | 0.000004135 | 84.1 |

$(B/A)_{MEAN}$ = 20324419. +/- 11305879.

A = 0.000003442 +/- 0.000000477 +/- 0.000001095

B = 70.0 +/- 9.7 +/- 61.3

MEAN ABSORPTION COEFICIENT = 87.80 +/- 27.95

UNCRUSHED MICROBEADS LESS 37 M

BRIGHTNESS EMISSIVITY = 1.00
MEAN EMISSIVITY = 1.00

| THICKNESS CMS | DENSITY $G/CMS^3$ | BATH TEMP | KINETIC TEMP | BRIGHTNESS TEMP | EFFECTIVE TEMP | A | B |
|---|---|---|---|---|---|---|---|
| 0.29 | 1.28 | 318.6 | 197.25 | 197.25 | 197.25 | 0.000006013 | 90.7 |
| | | 295.0 | 188.04 | 188.04 | 188.04 | 0.000006229 | 93.9 |
| | | 279.3 | 181.64 | 181.64 | 181.64 | 0.000006333 | 95.5 |
| 0.80 | 1.47 | 327.1 | 171.55 | 171.55 | 171.55 | 0.000007503 | 113.1 |
| | | 281.0 | 152.71 | 152.71 | 152.71 | 0.000006795 | 102.5 |
| | | 295.5 | 158.44 | 158.44 | 158.44 | 0.000007004 | 105.7 |
| 0.43 | 1.39 | 328.1 | 185.21 | 185.21 | 185.21 | 0.000005819 | 87.8 |
| | | 280.9 | 166.94 | 166.94 | 166.94 | 0.000005826 | 87.8 |
| | | 295.3 | 173.08 | 173.08 | 173.08 | 0.000005931 | 89.5 |
| 0.40 | 1.17 | 279.6 | 170.32 | 170.32 | 170.32 | 0.000006124 | 92.4 |
| | | 295.9 | 177.14 | 177.14 | 177.14 | 0.000006184 | 93.3 |
| | | 320.8 | 187.19 | 187.19 | 187.19 | 0.000006184 | 93.2 |

(B/A) MEAN = 15073589. +/- 8230749.

A = 0.000006326 +/- 0.000000514 +/- 0.000001773

B = 95.4 +/- 7.8 +/- 78.9

MEAN ABSORPTION COEFICIENT = 47.78 +/- 13.39

CRUSHED QUARTZ 74-44 M

BRIGHTNESS EMISSIVITY = 1.00
MEAN EMISSIVITY = 1.00

| THICKNESS CMS | DENSITY $G/CMS^3$ | BATH TEMP | KINETIC TEMP | BRIGHTNESS TEMP | EFFECTIVE TEMP | A | B |
|---|---|---|---|---|---|---|---|
| 0.35 | 1.22 | 316.8 | 213.93 | 213.93 | 213.93 | 0.000003994 | 318.8 |
| | | 295.5 | 202.84 | 202.84 | 202.84 | 0.000003695 | 294.8 |
| | | 280.5 | 195.79 | 195.79 | 195.79 | 0.000003569 | 285.0 |
| 0.54 | 1.46 | 340.0 | 214.11 | 214.11 | 214.11 | 0.000004910 | 391.6 |
| | | 276.9 | 188.39 | 188.39 | 188.39 | 0.000004545 | 362.5 |
| | | 295.1 | 194.65 | 194.65 | 194.65 | 0.000004470 | 356.8 |

$(B/A)_{MEAN}$ = 79729983. +/- 85835796.

A = 0.000004195 +/- 0.000000522 +/- 0.000003733

B = 334.9 +/- 42.0 +/- 658.7

MEAN ABSORPTION COEFICIENT = 72.03 +/- 64.10

CRUSHED QUARTZ LESS 74M

BRIGHTNESS EMISSIVITY = 1.00
MEAN EMISSIVITY = 1.00

| THICKNESS CMS | DENSITY $G/CMS^3$ | BATH TEMP | KINETIC TEMP | BRIGHTNESS TEMP | EFFECTIVE TEMP | A | B |
|---|---|---|---|---|---|---|---|
| 0.40 | 1.24 | 296.3 | 205.78 | 205.78 | 205.78 | 0.000006355 | 335.4 |
| | | 344.5 | 231.62 | 231.62 | 231.62 | 0.000007346 | 387.8 |
| | | 276.7 | 197.13 | 197.13 | 197.13 | 0.000006303 | 332.7 |
| 0.20 | 1.10 | 297.1 | 212.15 | 212.15 | 212.15 | 0.000003800 | 200.6 |
| | | 345.5 | 237.56 | 237.56 | 237.56 | 0.000004210 | 222.4 |
| | | 279.8 | 204.88 | 204.88 | 204.88 | 0.000003867 | 204.2 |



$(B/A)_{MEAN}$ = 52742188. +/- 33183501.

A = 0.000005312 +/- 0.000001535 +/- 0.000002474

B = 280.5 +/- 81.0 +/- 307.1

MEAN ABSORPTION COEFICIENT = 56.89 +/- 26.48

COMBINED QUARTZ DATA

BRIGHTNESS EMISSIVITY = 1.00
MEAN EMISSIVITY = 1.00

| THICKNESS CMS | DENSITY $G/CMS^3$ | BATH TEMP | KINETIC TEMP | BRIGHTNESS TEMP | EFFECTIVE TEMP | A | B |
|---|---|---|---|---|---|---|---|
| 0.35 | 1.22 | 316.8 | 213.93 | 213.93 | 213.93 | 0.000004627 | 306.6 |
| | | 295.5 | 202.84 | 202.84 | 202.84 | 0.000004299 | 285.1 |
| | | 280.5 | 195.79 | 195.79 | 195.79 | 0.000004172 | 276.6 |
| 0.54 | 1.46 | 340.0 | 214.11 | 214.11 | 214.11 | 0.000005655 | 374.9 |
| | | 276.9 | 188.39 | 188.39 | 188.39 | 0.000005320 | 352.4 |
| | | 295.1 | 194.65 | 194.65 | 194.65 | 0.000005215 | 345.5 |
| 0.40 | 1.24 | 296.3 | 205.78 | 205.78 | 205.78 | 0.000005312 | 352.3 |
| | | 344.5 | 231.62 | 231.62 | 231.62 | 0.000006258 | 414.9 |
| | | 276.7 | 197.13 | 197.13 | 197.13 | 0.000005238 | 347.3 |
| 0.20 | 1.10 | 297.1 | 212.15 | 212.15 | 212.15 | 0.000003181 | 211.0 |
| | | 345.5 | 237.56 | 237.56 | 237.56 | 0.000003591 | 238.3 |
| | | 279.8 | 204.88 | 204.88 | 204.88 | 0.000003219 | 213.6 |

$(B/A)_{MEAN}$ = 66236085. +/- 55369275.

A = 0.000004672 +/- 0.000000991 +/- 0.000003085

B = 309.9 +/- 65.7 +/- 463.7

MEAN ABSORPTION COEFICIENT = 64.67 +/- 42.71

CRUSHED MICROBEADS 74-44 M

BRIGHTNESS EMISSIVITY = 1.00
MEAN EMISSIVITY = 1.00

| THICKNESS CMS | DENSITY $G/CMS^3$ | BATH TEMP | KINETIC TEMP | BRIGHTNESS TEMP | EFFECTIVE TEMP | A | B |
|---|---|---|---|---|---|---|---|
| 0.42 | 0.72 | 296.3 | 184.21 | 184.21 | 184.21 | 0.000003621 | 183.1 |
| | | 332.6 | 196.70 | 196.70 | 196.70 | 0.000003628 | 183.5 |
| | | 276.5 | 176.75 | 176.75 | 176.75 | 0.000003554 | 179.9 |
| 0.34 | 0.58 | 296.3 | 184.30 | 184.30 | 184.30 | 0.000002936 | 148.6 |
| | | 343.0 | 202.56 | 202.56 | 202.56 | 0.000003122 | 157.9 |
| | | 276.4 | 178.05 | 178.05 | 178.05 | 0.000003010 | 152.1 |
| 0.28 | 0.86 | 295.7 | 198.30 | 198.30 | 198.30 | 0.000003703 | 187.4 |
| | | 341.6 | 219.88 | 219.88 | 219.88 | 0.000004061 | 205.5 |
| | | 276.5 | 189.29 | 189.29 | 189.29 | 0.000003554 | 179.8 |

(B/A) MEAN = 50529413. +/- 42344119.

A = 0.000003465 +/- 0.000000365 +/- 0.000002198

B = 175.3 +/- 18.6 +/- 258.1

MEAN ABSORPTION COEFICIENT = 87.20 +/- 55.29

CRUSHED HORNBLENDE  LESS 74 M

BRIGHTNESS EMISSIVITY = 1.00
MEAN EMISSIVITY = 1.00

| THICKNESS CMS | DENSITY $G/CMS^3$ | BATH TEMP | KINETIC TEMP | BRIGHTNESS TEMP | EFFECTIVE TEMP | A | B |
|---|---|---|---|---|---|---|---|
| 0.60 | 1.50 | 296.0 | 189.45 | 189.45 | 189.45 | 0.000016287 | 154.3 |
| | | 344.6 | 208.05 | 208.05 | 208.05 | 0.000014335 | 135.8 |
| | | 277.3 | 178.95 | 178.95 | 178.95 | 0.000015557 | 147.4 |
| 0.20 | 1.11 | 297.0 | 180.90 | 180.90 | 180.90 | 0.000004202 | 39.8 |
| | | 340.6 | 197.10 | 197.10 | 197.10 | 0.000003830 | 36.3 |
| | | 277.7 | 171.10 | 171.10 | 171.10 | 0.000004053 | 38.4 |

(B/A) MEAN = 9468714. +/- 432043.

A = 0.000009716 +/- 0.000006251 +/- 0.000000164

B = 92.0 +/- 59.2 +/- 5.8

MEAN ABSORPTION COEFICIENT = 31.14 +/- 0.54

CRUSHED OLIVINE  LESS 74 M

BRIGHTNESS EMISSIVITY = 1.00
MEAN EMISSIVITY = 1.00

| THICKNESS CMS | DENSITY $G/CMS^3$ | BATH TEMP | KINETIC TEMP | BRIGHTNESS TEMP | EFFECTIVE TEMP | A | B |
|---|---|---|---|---|---|---|---|
| 0.41 | 1.37 | 295.9 | 190.96 | 190.96 | 190.96 | 0.000012055 | 103.7 |
| | | 342.9 | 217.11 | 217.11 | 217.11 | 0.000012733 | 109.5 |
| | | 278.2 | 183.10 | 183.10 | 183.10 | 0.000012383 | 106.5 |
| 0.42 | 1.37 | 278.3 | 183.40 | 183.40 | 183.40 | 0.000012778 | 109.9 |
| | | 294.8 | 190.95 | 190.95 | 190.95 | 0.000012532 | 107.8 |
| | | 343.1 | 217.80 | 217.80 | 217.80 | 0.000013225 | 113.7 |

(B/A) MEAN = 8598622. +/- 4416233.

A = 0.000012614 +/- 0.000000395 +/- 0.000002228

B = 108.5 +/- 3.4 +/- 74.9

MEAN ABSORPTION COEFICIENT = 23.97 +/- 4.24

Part 3

The experimental results are recomputed using a mean emissivity of 0.95 and an effective 8 - 14 μ emissivity of 0.88 as described in Appendix 3. The experimental errors are clearly much greater than the small changes in the values of B/A, B and A.

UNCRUSHED MICROBEADS 840-590M

BRIGHTNESS EMISSIVITY = 0.88
MEAN EMISSIVITY = 0.98

| THICKNESS CMS | DENSITY $G/CMS^3$ | BATH TEMP | KINETIC TEMP | BRIGHTNESS TEMP | EFFECTIVE TEMP | A | B |
|---|---|---|---|---|---|---|---|
| 0.78 | 1.82 | 279.9 | 174.72 | 171.65 | 173.84 | 0.000031434 | -22.1 |
| | | 296.2 | 184.90 | 181.51 | 183.97 | 0.000031449 | -22.1 |
| | | 319.0 | 197.93 | 194.12 | 196.93 | 0.000030532 | -21.4 |
| 0.47 | 1.77 | 319.9 | 218.38 | 213.74 | 217.28 | 0.000029482 | -20.7 |
| | | 295.5 | 201.69 | 197.69 | 200.68 | 0.000029542 | -20.7 |
| | | 280.1 | 189.95 | 186.39 | 188.99 | 0.000028618 | -20.1 |
| 0.41 | 1.61 | 279.4 | 192.68 | 188.97 | 191.71 | 0.000027239 | -19.1 |
| | | 296.2 | 205.13 | 200.97 | 204.09 | 0.000027783 | -19.5 |
| | | 321.6 | 225.17 | 220.30 | 224.04 | 0.000029348 | -20.6 |
| 0.20 | 1.59 | 295.7 | 231.35 | 226.23 | 230.18 | 0.000027284 | -19.1 |
| | | 336.9 | 262.74 | 256.25 | 261.42 | 0.000026561 | -18.6 |
| | | 276.1 | 215.65 | 211.17 | 214.56 | 0.000027113 | -19.0 |
| 0.90 | 1.64 | 297.1 | 184.30 | 180.89 | 183.37 | 0.000035204 | -24.7 |
| | | 337.1 | 203.03 | 198.95 | 202.00 | 0.000030600 | -21.5 |
| | | 277.5 | 172.15 | 169.21 | 171.29 | 0.000035204 | -24.7 |

$(B/A)_{MEAN}$ = -701401. +/- 2116627.

A = 0.000029825 +/- 0.000002690 +/- 0.000004128

B = -20.9 +/- 1.9 +/- 60.2

MEAN ABSORPTION COEFICIENT = 10.14 +/- 1.40

UNCRUSHED MICROBEADS 350-250M

BRIGHTNESS EMISSIVITY = 0.88
MEAN EMISSIVITY = 0.98

| THICKNESS CMS | DENSITY $G/CMS^3$ | BATH TEMP | KINETIC TEMP | BRIGHTNESS TEMP | EFFECTIVE TEMP | A | B |
|---|---|---|---|---|---|---|---|
| 0.34 | 1.50 | 296.6 | 190.99 | 187.40 | 190.03 | 0.000014894 | 4.6 |
| | | 279.0 | 180.23 | 177.04 | 179.32 | 0.000014938 | 4.7 |
| | | 332.5 | 213.95 | 209.50 | 212.87 | 0.000015102 | 4.7 |
| 0.50 | 1.61 | 296.5 | 175.99 | 172.86 | 175.11 | 0.000014745 | 4.6 |
| | | 346.6 | 201.94 | 197.91 | 200.93 | 0.000013918 | 4.3 |
| | | 277.5 | 165.17 | 162.42 | 164.34 | 0.000014663 | 4.6 |

(B/A) MEAN = 311425. +/- 757430.

A = 0.000014707 +/- 0.000000417 +/- 0.000000715

B = 4.6 +/- 0.1 +/- 11.4

MEAN ABSORPTION COEFICIENT = 20.56 +/- 1.01

UNCRUSHED MICROBEADS 125-88 M

BRIGHTNESS EMISSIVITY = 0.88
MEAN EMISSIVITY = 0.98

| THICKNESS CMS | DENSITY $G/CMS^3$ | BATH TEMP | KINETIC TEMP | BRIGHTNESS TEMP | EFFECTIVE TEMP | A | B |
|---|---|---|---|---|---|---|---|
| 0.40 | 1.63 | 295.2 | 175.58 | 172.50 | 174.70 | 0.000009708 | 34.1 |
| | | 322.7 | 188.88 | 185.36 | 187.92 | 0.000009559 | 33.6 |
| | | 280.4 | 168.65 | 165.76 | 167.80 | 0.000009827 | 34.5 |
| 0.41 | 1.57 | 279.3 | 163.23 | 160.53 | 162.41 | 0.000008695 | 30.5 |
| | | 294.4 | 170.25 | 167.35 | 169.39 | 0.000008643 | 30.4 |
| | | 318.7 | 183.14 | 179.78 | 182.22 | 0.000008896 | 31.2 |

$(B/A)_{MEAN}$ = 3509437. +/- 2616892.

A = 0.000009224 +/- 0.000000529 +/- 0.000001378

B = 32.4 +/- 1.9 +/- 29.0

MEAN ABSORPTION COEFICIENT = 32.80 +/- 4.90

UNCRUSHED MICROBEADS 74-53 M

BRIGHTNESS EMISSIVITY = 0.88
MEAN EMISSIVITY = 0.98

| THICKNESS CMS | DENSITY $G/CMS^3$ | BATH TEMP | KINETIC TEMP | BRIGHTNESS TEMP | EFFECTIVE TEMP | A | B |
|---|---|---|---|---|---|---|---|
| 0.20 | 1.68 | 296.3 | 188.95 | 185.43 | 188.00 | 0.000003614 | 73.5 |
| | | 333.4 | 206.85 | 202.66 | 205.81 | 0.000003815 | 77.7 |
| | | 277.5 | 180.78 | 177.52 | 179.87 | 0.000003584 | 72.9 |
| 0.20 | 1.38 | 297.3 | 185.23 | 181.80 | 184.30 | 0.000003204 | 65.2 |
| | | 346.1 | 205.80 | 201.65 | 204.76 | 0.000003248 | 66.1 |
| | | 277.2 | 176.05 | 172.91 | 175.16 | 0.000003099 | 63.1 |
| 0.40 | 1.60 | 296.2 | 171.95 | 169.03 | 171.08 | 0.000004373 | 88.9 |
| | | 343.1 | 186.46 | 183.06 | 185.52 | 0.000004083 | 83.1 |
| | | 277.1 | 165.54 | 162.75 | 164.71 | 0.000004433 | 90.2 |

(B/A) MEAN = 20333477. +/- 11928417.

A = 0.000003718 +/- 0.000000492 +/- 0.000001237

B = 75.7 +/- 10.1 +/- 69.6

MEAN ABSORPTION COEFICIENT = 81.32 +/- 27.10

UNCRUSHED MICROBEADS LESS 37 M

BRIGHTNESS EMISSIVITY = 0.88
MEAN EMISSIVITY = 0.98

| THICKNESS CMS | DENSITY $G/CMS^3$ | BATH TEMP | KINETIC TEMP | BRIGHTNESS TEMP | EFFECTIVE TEMP | A | B |
|---|---|---|---|---|---|---|---|
| 0.29 | 1.28 | 318.6 | 201.19 | 197.25 | 200.18 | 0.000006557 | 98.3 |
| | | 295.0 | 191.62 | 188.04 | 190.65 | 0.000006780 | 101.7 |
| | | 279.3 | 185.05 | 181.64 | 184.12 | 0.000006899 | 103.5 |
| 0.80 | 1.47 | 327.1 | 174.61 | 171.55 | 173.73 | 0.000008032 | 120.4 |
| | | 281.0 | 155.19 | 152.71 | 154.41 | 0.000007249 | 108.8 |
| | | 295.5 | 161.07 | 158.44 | 160.25 | 0.000007473 | 112.1 |
| 0.43 | 1.39 | 328.1 | 188.70 | 185.21 | 187.75 | 0.000006273 | 94.1 |
| | | 280.9 | 169.89 | 166.94 | 169.03 | 0.000006273 | 94.1 |
| | | 295.3 | 176.14 | 173.08 | 175.25 | 0.000006385 | 95.7 |
| 0.40 | 1.17 | 279.6 | 173.31 | 170.32 | 172.44 | 0.000006601 | 99.1 |
| | | 295.9 | 180.34 | 177.14 | 179.44 | 0.000006676 | 100.1 |
| | | 320.8 | 190.75 | 187.19 | 189.79 | 0.000006683 | 100.2 |

(B/A) MEAN = 14990467. +/- 8521224.

A = 0.000006825 +/- 0.000000522 +/- 0.000001967

B = 102.3 +/- 7.9 +/- 87.7

MEAN ABSORPTION COEFICIENT = 44.32 +/- 12.80

CRUSHED QUARTZ 74-44 M

BRIGHTNESS EMISSIVITY = 0.88
MEAN EMISSIVITY = 0.98

| THICKNESS CMS | DENSITY $G/CMS^3$ | BATH TEMP | KINETIC TEMP | BRIGHTNESS TEMP | EFFECTIVE TEMP | A | B |
|---|---|---|---|---|---|---|---|
| 0.35 | 1.22 | 316.8 | 218.60 | 213.93 | 217.49 | 0.000004478 | 355.3 |
| | | 295.5 | 207.06 | 202.84 | 206.01 | 0.000004128 | 327.6 |
| | | 280.5 | 199.73 | 195.79 | 198.72 | 0.000003986 | 316.5 |
| 0.54 | 1.46 | 340.0 | 218.70 | 214.11 | 217.60 | 0.000005439 | 431.7 |
| | | 276.9 | 192.02 | 188.39 | 191.05 | 0.000005029 | 399.1 |
| | | 295.1 | 198.53 | 194.65 | 197.53 | 0.000004947 | 392.7 |

(B/A) = 79341284. +/- 85854599.
MEAN

A = 0.000004664 +/- 0.000000559 +/- 0.000004157

B = 370.5 +/- 44.8 +/- 730.9

MEAN ABSORPTION COEFICIENT = 64.79 +/- 57.70

CRUSHED QUARTZ LESS 74M

BRIGHTNESS EMISSIVITY = 0.88
MEAN EMISSIVITY = 0.98

| THICKNESS CMS | DENSITY $G/CMS^3$ | BATH TEMP | KINETIC TEMP | BRIGHTNESS TEMP | EFFECTIVE TEMP | A | B |
|---|---|---|---|---|---|---|---|
| 0.40 | 1.24 | 296.3 | 210.10 | 205.78 | 209.05 | 0.000006266 | 387.3 |
| | | 344.5 | 237.01 | 231.62 | 235.81 | 0.000007384 | 456.4 |
| | | 276.7 | 201.06 | 197.13 | 200.04 | 0.000006177 | 381.8 |
| 0.20 | 1.10 | 297.1 | 216.67 | 212.15 | 215.58 | 0.000003770 | 233.3 |
| | | 345.5 | 243.21 | 237.56 | 241.98 | 0.000004262 | 263.6 |
| | | 279.8 | 209.18 | 204.88 | 208.13 | 0.000003837 | 237.5 |

(B/A) MEAN = 61784763. +/- 47713197.

A = 0.000005282 +/- 0.000001520 +/- 0.000003114

B = 325.6 +/- 94.0 +/- 445.1

MEAN ABSORPTION COEFICIENT = 57.23 +/- 33.78

COMBINED QUARTZ DATA

BRIGHTNESS EMISSIVITY = 0.88
MEAN EMISSIVITY = 0.98

| THICKNESS CMS | DENSITY $G/CMS^3$ | BATH TEMP | KINETIC TEMP | BRIGHTNESS TEMP | EFFECTIVE TEMP | A | B |
|---|---|---|---|---|---|---|---|
| 0.35 | 1.22 | 316.8 | 218.60 | 213.93 | 217.49 | 0.000004910 | 346.7 |
| | | 295.5 | 207.06 | 202.84 | 206.01 | 0.000004545 | 320.8 |
| | | 280.5 | 199.73 | 195.79 | 198.72 | 0.000004396 | 310.7 |
| 0.54 | 1.46 | 340.0 | 218.70 | 214.11 | 217.60 | 0.000005946 | 420.0 |
| | | 276.9 | 192.02 | 188.39 | 191.05 | 0.000005551 | 392.1 |
| | | 295.1 | 198.53 | 194.65 | 197.53 | 0.000005454 | 384.9 |
| 0.40 | 1.24 | 296.3 | 210.10 | 205.78 | 209.05 | 0.000005633 | 397.8 |
| | | 344.5 | 237.01 | 231.62 | 235.81 | 0.000006706 | 473.5 |
| | | 276.7 | 201.06 | 197.13 | 200.04 | 0.000005536 | 390.7 |
| 0.20 | 1.10 | 297.1 | 216.67 | 212.15 | 215.58 | 0.000003397 | 239.9 |
| | | 345.5 | 243.21 | 237.56 | 241.98 | 0.000003874 | 273.8 |
| | | 279.8 | 209.18 | 204.88 | 208.13 | 0.000003442 | 243.4 |

$(B/A)_{MEAN}$ = 70563023. +/- 57607270.

A = 0.000004947 +/- 0.000001036 +/- 0.000003219

B = 349.5 +/- 73.1 +/- 512.6

MEAN ABSORPTION COEFICIENT = 61.08 +/- 39.72

CRUSHED MICROBEADS 74-44 M

BRIGHTNESS EMISSIVITY = 0.88
MEAN EMISSIVITY = 0.98

| THICKNESS CMS | DENSITY $G/CMS^3$ | BATH TEMP | KINETIC TEMP | BRIGHTNESS TEMP | EFFECTIVE TEMP | A | B |
|---|---|---|---|---|---|---|---|
| 0.42 | 0.72 | 296.3 | 187.67 | 184.21 | 186.72 | 0.000004008 | 197.9 |
| | | 332.6 | 200.67 | 196.70 | 199.66 | 0.000004023 | 198.5 |
| | | 276.5 | 180.00 | 176.75 | 179.10 | 0.000003949 | 194.8 |
| 0.34 | 0.58 | 296.3 | 187.77 | 184.30 | 186.83 | 0.000003256 | 160.7 |
| | | 343.0 | 206.74 | 202.56 | 205.70 | 0.000003465 | 171.1 |
| | | 276.4 | 181.28 | 178.05 | 180.36 | 0.000003338 | 164.5 |
| 0.28 | 0.86 | 295.7 | 202.29 | 198.30 | 201.27 | 0.000004165 | 205.5 |
| | | 341.6 | 224.79 | 219.88 | 223.65 | 0.000004582 | 226.1 |
| | | 276.5 | 192.94 | 189.29 | 191.97 | 0.000003994 | 197.0 |

(B/A) = 49276661. +/- 40523965.
MEAN

A = 0.000003867 +/- 0.000000425 +/- C.000002377

B = 190.7 +/- 21.2 +/- 274.2

MEAN ABSORPTION COEFICIENT = 78.19 +/- 48.12

## Appendix 5

## CONTACT CONDUCTION

The radius of the circle of contact formed between two elastic spheres under a compressive force was derived by Hertz (1895). He assumed that the radius of the spheres was very large compared with the contact radius and that the deformation was purely elastic and compressional. If $a$ is the radius of the contact and $\nu$ and $E$, Poisson's ratio and Young's modulus for the material, then the equation for the radius of the circle of contact between two spheres of radii $b$ under a compression force $P$ is

$$a^3 = \frac{3}{4} \frac{Pb(1 - \nu^2)}{E}$$

For silica glass (Birch, 1942)

$$E = 7 \times 10^{11} \text{ dynes/cm}^2$$

$$\nu = 0.18$$

$$\therefore \quad a^3 = 1.0 \times 10^{-12} Pb$$

If the compressive force $P$ is due to the weight of $m$ spheres above the contact then

$$P = m\rho \frac{4}{3} \pi b^3 g$$

where

$$\rho = 2.5 \text{ gms/cm}^3 \qquad \text{(glass density)}$$

$$g = 980 \text{ dynes/gm}$$

Hence

$$a_m^3 = 1 \times 10^{-8}\, mb^4$$

Now the contact resistance between two bodies of material resistivity $\tau$ with a contact area $\pi c^2$ is $\tau/2c$ provided that the contact is welded.

It was shown previously that the solid conduction term for powders cannot be explained by assuming that the reduction in conductivity from that of the solid is due to the lower density. This discussion will now proceed on the assumption that the low conductivity is due primarily to the high resistance of the contacts. It will also be assumed for the purposes of discussion that the powder can be idealized by cubic packing.

Consider a three-dimensional mesh of resistances whose individual resistances are constant at any level but increase in depth. Suppose that there are $m$ resistances in a column and $n^2$ resistances in a layer.

The resistance of a single layer $K$ is due to $n^2$ resistances of equal value $r_K$ in parallel.

$$\therefore \frac{1}{dR_K} = \frac{n^2}{r_K}$$

The total resistance of the mesh is the sum of $m$ levels in series.

$$R_T = \sum_{K=1}^{m} dR_K = \frac{1}{n^2} \sum_{K=1}^{m} r_K$$

The contact resistance $r_K$ is chosen as the contact resistance between spheres of radius $b$ and contact area $\pi a_K^2$ where $a_K$ is

derived for a compressive force due to K spheres.

$$\therefore\ r_K = \tau/2a_K$$

Let $n = 1/2b$ and $m = L/2b$ where L is the sample thickness.

$$\therefore\ R_T = \frac{4b^2\tau}{2} \sum_{K=1}^{L/2b} \frac{1}{a_K}$$

and

$$a_K = 10^{-8/3} K^{1/3} b^{4/3}$$

thus

$$R_T = 2b^{2/3} 10^{8/3} \tau \sum_{K=1}^{L/2b} K^{-1/3}$$

Now the resistance of a block with unit cross-sectional area, thickness L and resistivity $\tau$ is

$$R_B = \tau L$$

$$\therefore\ \frac{R_T}{R_B} = \frac{2b^{2/3} 10^{8/3}}{L} \sum_{K=1}^{L/2b} K^{-1/3}$$

Since the conductivity of glass is approximately $10^5$ ergs/cm/sec/deg then the theoretical powder conductivity should be given by

$$K_P = \frac{R_B}{R_T} \times 10^5 = \frac{10^{7/3} L b^{-2/3}}{2 \sum_{K=1}^{L/2b} K^{-1/3}}$$

Numerical Results

| Grain Size (Microns) | K (ergs/cm/sec/deg) L = 0.2 cm | L = 0.5 cm | L = 1.0 cm |
|---|---|---|---|
| 1000 | 89 | 107 | 128 |
| 200 | 75 | 97 | 119 |
| 100 | 72 | 94 | 117 |
| 50 | 70 | 93 | 116 |

Essentially then, the welded elastic contact theory implies that the conductivity of the powder should be reasonably insensitive to grain sizes over the range of powders examined in this study. The fact that this is not confirmed by the experimental results for the uncrushed glass spheres suggests that this idealized model is incorrect.

If we assume that $r_K$ is independent of the compressive load and the grain size then

$$K_P = \frac{a}{b} \times 10^5$$

where $\pi a^2$ is an effective contact area. A crude fit to the contact conduction of the glass spheres is $K_P = 3000/2b$, where $K_P$ is in ergs/cm$^2$/sec and b is in microns.

$$\therefore a \sim 1.5 \times 10^{-2} \text{ microns}$$

Recall from Hertz' theory that for a sample thickness of 0.2 cm above a sphere-sphere contact

$$a^3 \sim 10^{-9} b^3$$

$$\therefore \quad a \sim 10^{-3} b$$

$$\begin{cases} \text{if } b = 100\ \mu, & a = 0.1\ \mu \\ b = 50\ \mu, & a = 0.05\ \mu \end{cases}$$

It is clear that agreement between the magnitude of the conductivity for the welded elastic contact model and the glass spheres probably should not be expected. However the differences in the grain size dependence are surprising. The results suggest that the thermal contact may be unrelated in any simple sense to the elastic contact. The microscopic roughness of the contacting surfaces and the possible presence of a thin surface film on the glass spheres will cause departures from the welded contact model.

Appendix 6

# THE SOLUTION WITH CONSTANT THERMAL PROPERTIES

1) Wesselink's Solution (Wesselink, 1948)

Consider a half space which satisfies the assumptions of the models (infinite optical depth below the surface, unit emissivity, and constant thermal properties).

$$\frac{1}{\kappa} \cdot \frac{\partial T}{\partial t} = \frac{\partial^2 T}{\partial x^2}$$

Subject to the radiation boundary condition

$$k \frac{\partial T}{\partial x}\bigg|_{a=0} = - A + \sigma T_o^4$$

where $A$ is the insolation.

If $x$ is replaced by the parameter $\epsilon$ which is defined:

$$\epsilon = x/\ell$$

where

$$\ell = 2\sqrt{\pi \kappa \tau}$$ heat wavelength

$\tau$ = period of the insolation.

and the partial derivatives are replaced by first order finite differences, then the solution is relatively simple if $\Delta\epsilon$ and $\Delta t$ are chosen in the following manner

$$\frac{1}{4\pi\tau} \frac{\Delta t}{(\Delta\epsilon)^2} = \frac{1}{2}$$

The heat conduction equation is replaced by

$$T_m^{n+1} = \frac{1}{2}(T_{m-1}^n + T_{m+1}^n)$$

where

$$T_m^n \equiv T(\epsilon = m\Delta\epsilon + \epsilon_o,\ t = n\Delta t)$$

The boundary condition is reduced to a simple form by setting $\epsilon_o = -\frac{1}{2}\Delta\epsilon$ and defining a fictitious temperature at $m = 0$. The surface temperature is then taken as the mean between $m = 0$ and $m = 1$. Thus the surface boundary condition can be written

$$\sigma(S^{n+1})^4 = A + \frac{1}{P\Delta\epsilon\sqrt{\pi\tau}}\,(T_1^{n+1} - S^{n+1})$$

where $S^{n+1}$ represents the surface temperature and $P = (k\rho c)^{-1/2}$ is called the thermal inertia.

The solution for the surface temperature is completely specified by the period $\tau$, the thermal inertia $P$, and the insolation $A$. When the thermal properties are not independent of temperature then $P$ cannot be regarded as a useful parameter since the surface temperature depends on specifying both the specific heat and the thermal conductivity.

2) Jaeger's Solution (1953 b)

The solution is constructed by assuming a periodic step function for the surface temperature and computing the average flux into the solid in each interval. This flux is computed for steady conditions using the method of Laplace Transforms.

$$F_n = \frac{1}{P\sqrt{\pi\tau}} \sum_{s=1}^{N} T_s \phi_{n-s+1}$$

where $F_n$ is the flux into the solid in the nth interval and the coefficients

$$\phi_1 = 2\sqrt{N} - \frac{2N}{\sqrt{\pi}} \int_o^\infty \frac{(1 - e^{-x^2/N})[\, e^{-(n-1)x^2/N} - e^{-x^2}\,]\, dx}{x^2(1 - e^{-x^2})}$$

$$\phi_n = 2[\, \sqrt{n} + \sqrt{n-2} - 2\sqrt{n-1}\,]\sqrt{N}$$

$$- \frac{2N}{\sqrt{\pi}} \int_o^\infty \frac{e^{-(n-1)x^2/N}(1 - e^{-x^2/N})(e^{-(N-1)x^2/N} - e^{-x^2})\, dx}{x^2(1 - e^{-x^2})}$$

$$n = 2,\ 3,\ \ldots\ ,\ N$$

The boundary condition is

$$F_n = A_n - \sigma T_n^4$$

where $A_n$ is the insolation.

An initial guess is made of the surface temperature, and the resulting flux is computed. A new set of surface temperatures are then determined from the boundary condition.

Jaeger has computed the solution for $N = 20$, which was adequate for his comparison with the subsolar and midnight temperatures observed by Pettit and Nicholson. A solution for $N = 200$ was computed by this author to provide a comparison with the Schmidt method solution used by Wesselink and the author's solution. No difference between the surface temperatures of the three models exceeded 0.5°K for $P = 1000$.